NUWC-NPT Technical Report 11,820
25 June 2007

Quadrifilar Helical Antenna Array for Line-of-Sight Communications Above the Ocean Surface

Michael J. Josypenko
John P. Casey
Stephen M. Davis
Undersea Warfare Electromagnetic Systems Department

Naval Undersea Warfare Center Division
Newport, Rhode Island

PREFACE

This report was prepared under the NUWC Independent Applied Research (IAR) Program, Project No. G62201, "Multipath-Abating Antenna System for High Data Rate Communications with the Undersea Grid," program manager Richard B. Philips (Code 01CTO). The sponsoring activity is the Office of Naval Research.

The technical reviewer for this report was Paul Medeiros (Code 3413).

The authors are grateful to Paul Medeiros (Code 3413) for his technical guidance and to Donald H. Steinbrecher (Code 3404) for his suggestion of this project. The authors also wish to thank Matthew W. Atwood (Code 3433) for his design of the collar that attached the array to the buoy plate and for his design of the rack that mounted the amplifiers and filters to the buoy plate. The authors acknowledge Jeremy M. Smith of Anteon Corp. for his mechanical assembly of the antenna support structures.

Reviewed and Approved: 25 June 2007

Gerald M. Exley
Head, Undersea Warfare Electromagnetic Systems Department

REPORT DOCUMENTATION PAGE

Form Approved
OMB No. 0704-0188

1. AGENCY USE ONLY *(Leave blank)*	2. REPORT DATE	3. REPORT TYPE AND DATES COVERED
	25 June 2007	

4. TITLE AND SUBTITLE

Quadrifilar Helical Antenna Array for Line-of-Sight Communications Above the Ocean Surface

5. FUNDING NUMBERS

6. AUTHOR(S)

Michael J. Josypenko, John P. Casey, Stephen M. Davis

7. PERFORMING ORGANIZATION NAME(S) AND ADDRESS(ES)

Naval Undersea Warfare Center Division
1176 Howell Street
Newport, RI 02841-1708

8. PERFORMING ORGANIZATION REPORT NUMBER

TR 11,820

9. SPONSORING/MONITORING AGENCY NAME(S) AND ADDRESS(ES)

Office of Naval Research
875 North Randolph Street
Suite 1425
Arlington VA 22203-1995

10. SPONSORING/MONITORING AGENCY REPORT NUMBER

11. SUPPLEMENTARY NOTES

12a. DISTRIBUTION/AVAILABILITY STATEMENT

Approved for public release; distribution is unlimited.

12b. DISTRIBUTION CODE

13. ABSTRACT (Maximum 200 words)

This report describes the development of a linear array consisting of four quadrifilar helical antennas (QHAs) that is mounted on a buoy to support transmit and receive communications at 2.45 GHz along line-of-sight (LOS) paths above a sea water half-space. The array elements are designed to be immune to the multipath interference created by reflections of an incident signal from the surface of the ocean. A novel feed design for the array is described. The circuit and radiation characteristics of each QHA element measured in free space are presented. The predicted radiation pattern of each QHA element at its nominal height above a flat ocean surface is determined from the measured element pattern in free space.

14. SUBJECT TERMS

Quadrifilar Helix, Multipath, Cut-in Frequency, VSWR, Pattern Front-to-Back Ratio, Bifilar Helix, Turnstile Antenna

15. NUMBER OF PAGES
76

16. PRICE CODE

17. SECURITY CLASSIFICATION OF REPORT	18. SECURITY CLASSIFICATION OF THIS PAGE	19. SECURITY CLASSIFICATION OF ABSTRACT	20. LIMITATION OF ABSTRACT
Unclassified	Unclassified	Unclassified	Unclassified

TABLE OF CONTENTS

LIST OF ILLUSTRATIONS

LIST OF ILLUSTRATIONS (Cont'd)

LIST OF ILLUSTRATIONS (Cont'd)

LIST OF ILLUSTRATIONS (Cont'd)

Figure **Page**

LIST OF TABLES

Table **Page**

LIST OF ABBREVIATIONS AND ACRONYMS

GPS	Global Positioning System
IAR	Independent Applied Research
LHCP	Left-hand circularly polarized
LOS	Line-of-sight
LPF	Low-pass filter
NEC	Numerical Electromagnetics Code
NUWC	Naval Undersea Warfare Center
QHA	Quadrifilar helical antenna
RF	Radio frequency
RHCP	Right-hand circularly polarized
VSWR	Voltage standing wave ratio

QUADRIFILAR HELICAL ANTENNA ARRAY FOR LINE-OF-SIGHT COMMUNICATIONS ABOVE THE OCEAN SURFACE

1. INTRODUCTION

Consider an antenna located above the ocean surface that is used for the transmission and reception of radio signals along line-of-sight (LOS) paths as shown in figure 1-1. For simplicity, a flat sea surface is assumed. Signal transmission and reception occur via two primary paths, i.e., the direct path and the sea water reflected path. Because these two paths are of different lengths, the signals associated with them arrive with different phases. The signals from the direct and reflected paths might arrive in phase, resulting in constructive interference and an increase in total signal amplitude by as much as 6 dB above the free-space value. Alternatively, the two signals may arrive out of phase, resulting in destructive interference and a decrease in total signal amplitude. The reduction in signal strength can be very large if the two signals are nearly equal in amplitude and 180° out of phase. Because of the dynamic sea state, the difference in length of the direct and reflected paths varies with time. Therefore, to reduce the probability of intermittent loss of signal, the antenna system should be designed to be immune to the reflected-path signal.

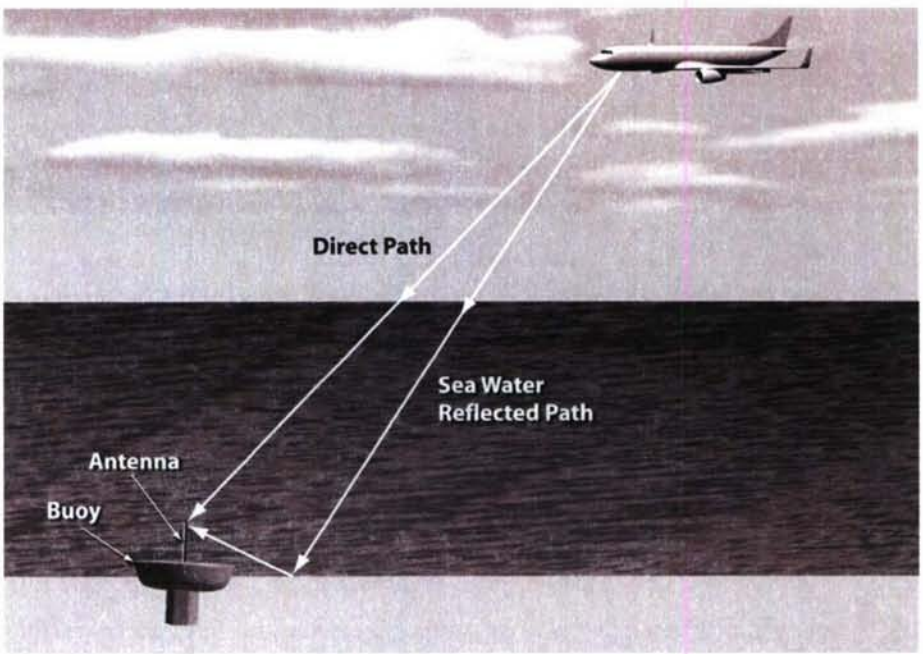

Figure 1-1. Line-of-Sight Communications in an Ocean Environment

The objective of this project is to develop a short, three- to four-element vertically-stacked antenna array and array-signal processor system that is installed on a buoy and is capable of supporting the transmission and reception of information at high data rates along LOS paths above an air-sea water interface. The operating frequency chosen for this antenna system is 2.45 GHz (reference 1) with a narrow instantaneous bandwidth. Over this frequency band, the ideal array elements should be circularly polarized with hemispherical radiation patterns in the upper half-space. In addition, each element should have significantly less gain in the lower half-space to minimize the amplitude of the reflected signal. The antenna elements should not couple significantly to sea water so that the impedance and radiation characteristics of the array are fairly immune to buoy motion and sea state. The array must attach to a mast that extends above the buoy (figure 1-2), have a length of no greater than 18 in., and should be able to withstand buoy tilt up to approximately 20° from the vertical position. To reduce the probability of washover, the array is separated from the top surface of the buoy by approximately 12 in. Several antennas were investigated to determine if they can meet the above requirements.

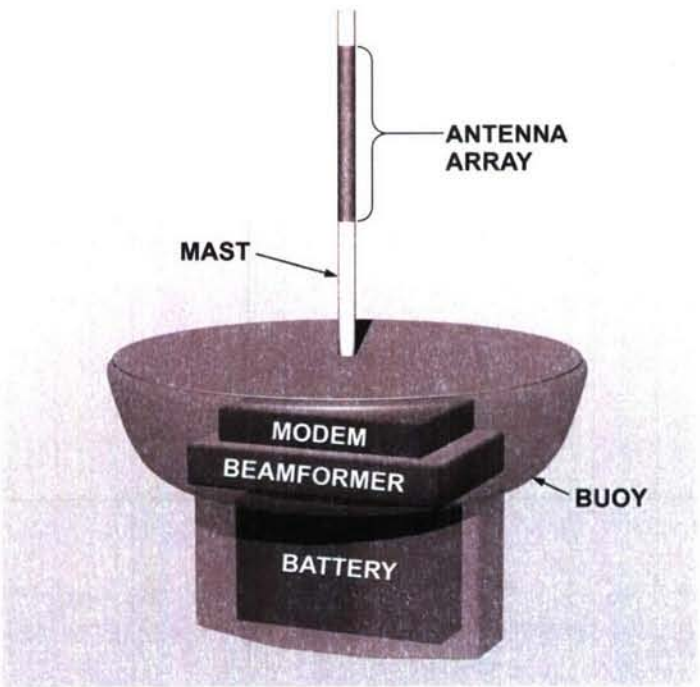

Figure 1-2. Conceptual View of Multipath-Abating Antenna System Installed on a Buoy

In this report, the results of an analysis of two candidate antenna arrays are presented and compared. A detailed description of the chosen antenna design and the measured circuit and radiation characteristics of each array element are presented. A description and analysis of the entire antenna system is given in another report by the authors (reference 1).

2. ANALYSIS OF SEVERAL CANDIDATE ANTENNAS

At the outset of this project, several possible antenna designs were considered that might provide both hemispherical coverage and immunity with respect to the signal reflected from the ocean surface. Although a gimbaled reflector antenna system would be a suitable candidate for this application, the high cost associated with the gimbal system is prohibitive. Two candidate antenna systems considered in this investigation were a turnstile array and a quadrifilar helical antenna (QHA) array. This section provides a summary of these investigations.

2.1 TURNSTILE ANTENNA ARRAY

The turnstile antenna (references 2 and 3) consists of two center-fed dipoles that are perpendicular to each other, with their axes intersecting at their midpoints. The dipoles are fed 90° out of phase with equal excitation voltages, resulting in a nearly omnidirectional radiation pattern with circular polarization in the direction perpendicular to the plane of the dipoles. Consequently, the dipole current distributions are equal in magnitude and 90° out of phase with respect to each other.

Counselman (reference 4) has developed several turnstile antenna array designs for the L1 and L2 Global Positioning System (GPS) frequency bands that have a fairly constant gain in the upper hemisphere and significantly less gain in the lower half-space. Counselman obtained this performance through a careful design of the array feed network and an optimum choice of element excitations or weights. One of Counselman's turnstile antenna array designs, consisting of 11 elements (separate elements used at each GPS frequency), was analyzed through use of the Numerical Electromagnetics Code (NEC), Version 4.1 (reference 5). The NEC model used in the analysis of this array was obtained from Counselman (reference 6).

Figure 2-1 illustrates a thin-wire model of an 11-element, dual-band turnstile antenna array obtained from Counselman (reference 6). In this design, five turnstile elements are used in the L1 GPS band (center frequency = 1575.42 MHz) and six turnstile elements are used in the L2 GPS band (center frequency = 1227.6 MHz). The element locations and weights are given in

table 2 of reference 4. In this design, each turnstile antenna element consists of four coplanar and mutually perpendicular monopoles that are fed in time-phase quadrature, a design that is equivalent to the two-dipole turnstile discussed earlier. Each monopole extends horizontally from a center post, which both mechanically supports the monopoles and contains the transmission lines that feed them. The center post extends approximately 36.19-in. long and includes four 1.0-in. wide radial blade conductors that intersect along the array axis at right angles. The radial blades serve as ground planes for the monopole elements. In the thin-wire model of the turnstile array, the radial blades are represented by wire grids (reference 6).

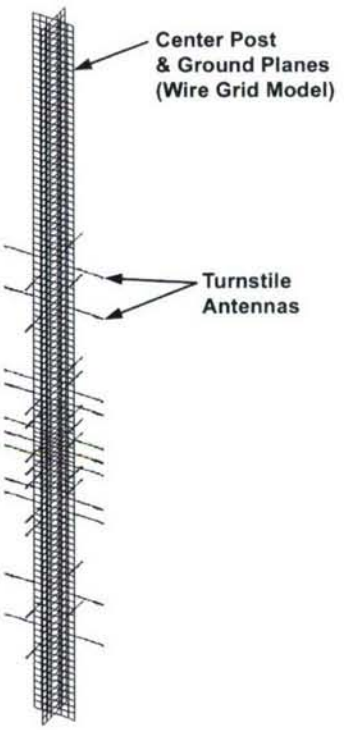

Figure 2-1. Thin-Wire Model of Eleven-Element Turnstile Antenna Array Used for GPS Applications as Obtained from Counselman (Reference 6)

The turnstile array in figure 2-1 uses separate arrays for the L1 and L2 GPS bands because of the difference in the wavelengths at these frequencies. The electrical length of each array is 2λ, where the physical lengths of the L1 and L2 arrays are 0.38 m and 0.488 m, respectively. In addition, the elements in each array are uniformly spaced by $\lambda/3$ at their respective center frequencies. The phase center of each turnstile element is coincident with its geometrical center, and the phase centers of the two arrays are located at the same point.

Figure 2-2 shows the computed directive gain patterns of the Counselman turnstile array in figure 2-1 at the L1 and L2 band center frequencies in free space and at various heights h above sea water. The free-space patterns are approximately hemispherical overhead with a maximum gain in the axial direction. In addition, the free-space patterns show very little radiation in the lower half-space. Consequently, the radiation pattern in the upper half-space should change very little when the array is located above sea water. In figure 2-2, the radiation patterns of the turnstile array above sea water are nearly identical to the free-space pattern except at small elevation angles where multipath interference of as much as 3 dB is observed. The small amount of multipath interference observed on these plots suggests that Counselman's array is immune to multipath interference.

Because the array is to be installed on a buoy that floats above a dynamic sea surface (figure 1-1), the effect of buoy tilt on the radiation pattern must be examined. Figure 2-3 gives the computed directive gain patterns of the Counselman turnstile array tilted at 20° with respect to the vertical direction at the L1 band center frequency in free space and at various heights h above sea water. The tilt of the antenna results in a significant increase in the free-space gain in the lower half-space over a 20° region extending from 90° to 110° and a noticeable decrease in the free-space gain over the region extending from 270° to 290° as indicated in the free-space pattern in figure 2-3. Therefore, the Counselman array produces a large pattern front-to-back ratio (i.e., the ratio of the total gain along the forward and backward axial directions) only when it is oriented vertically. In figure 2-3, the patterns over sea water show an overall reduction in gain as well as substantial multipath interference at the lower elevation angles, especially over the region extending from 270° to 290° (opposite to the direction of tilt) where the direct field amplitude has significantly decreased and the reflected field amplitude has increased.

(a)

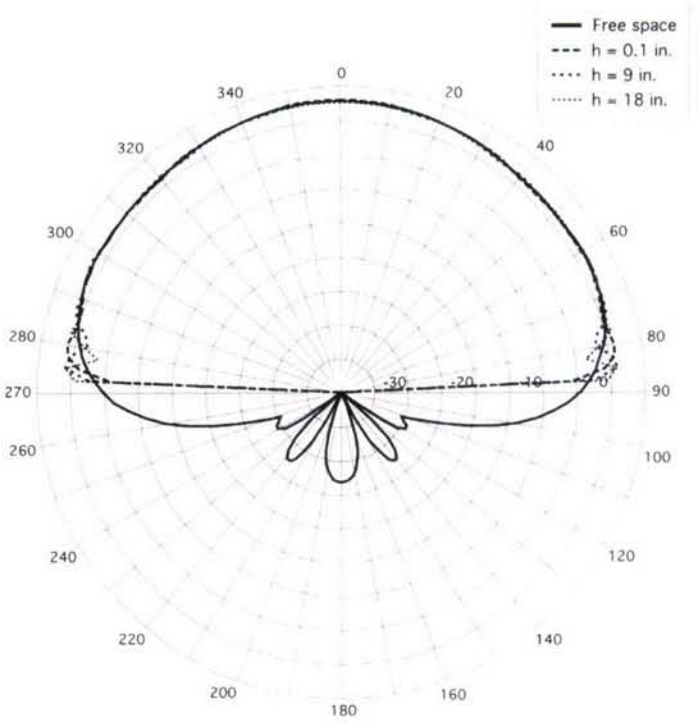

(b)

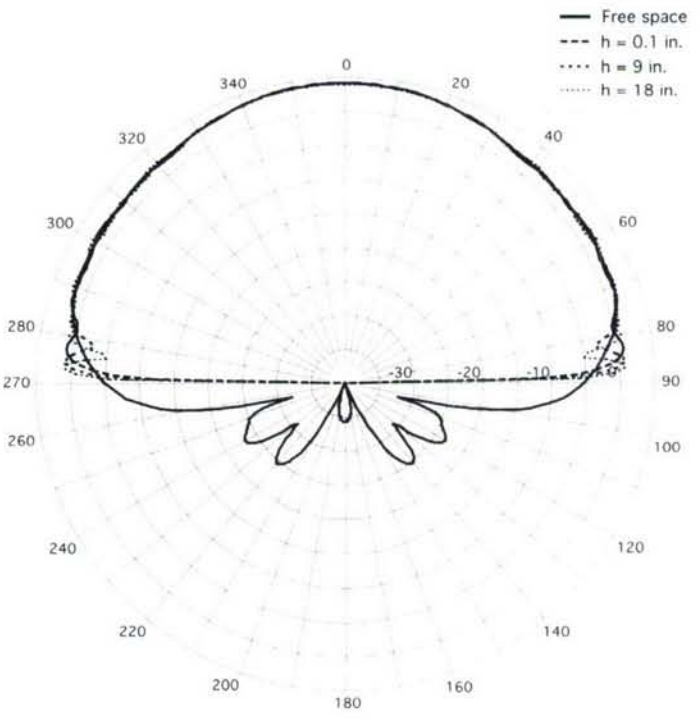

Figure 2-2. Computed Directive Gain Patterns (dB) in the Vertical Plane of the Counselman Turnstile Array (Figure 2-1) in Free Space and at Various Base Heights Above Sea Water: (a) 1227.6 MHz and (b) 1575.42 MHz

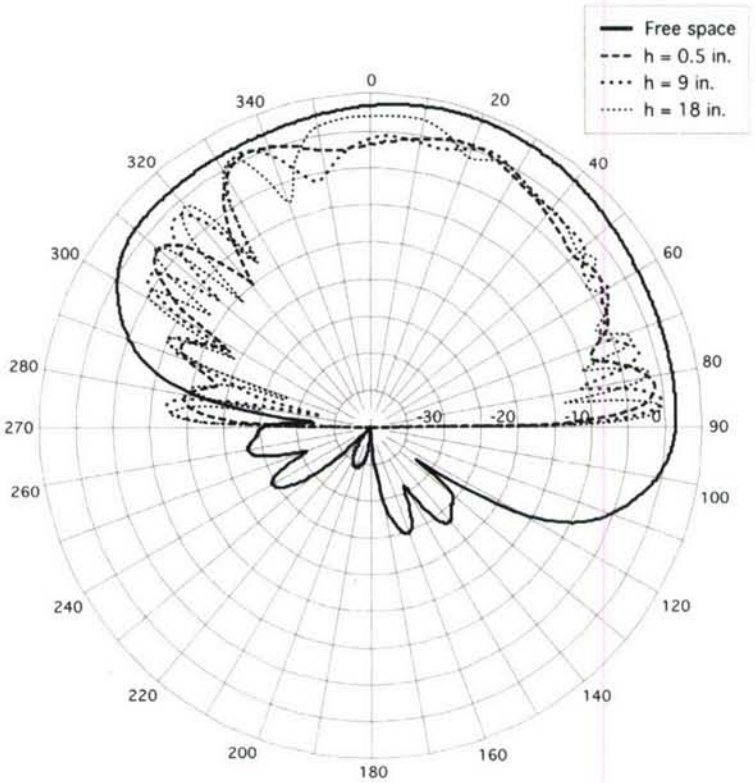

Figure 2-3. Computed Directive Gain Patterns (dB) in the Vertical Plane at 1575.42 MHz of the Counselman Turnstile Array (Figure 2-1) Tilted at 20° with Respect to the Vertical Direction in Free Space and at Various Base Heights Above Sea Water

In figure 2-3, note that the null depths associated with the multipath interference become deeper as the base height above sea water increases. If the tilt angle of the array is increased, the multipath interference will also intensify. Results similar to those in figure 2-3 were obtained at the L2 band center frequency.

The analysis of the turnstile array revealed the following problems:

1. The turnstile elements produce considerable radiation incident into the lower half-space. Therefore, the radiation pattern of the turnstile array is very sensitive to the array orientation relative to the ground plane. The large pattern front-to-back ratio observed for the Counselman array when oriented vertically with respect to the ocean surface is attributed to an optimum weighting of the turnstile elements. Any variation in the orientation of the array with respect to the sea water surface will produce a change in the element radiation characteristics with

increased multipath interference. As a result, unless the element weights are modified dynamically to account for antenna movement associated with sea state, the turnstile array is quite susceptible to multipath interference.

2. A dipole antenna generally couples to nearby structures that are located close to its axis. Therefore, if the turnstile array is close to the sea surface, the elements located closest to the sea surface (i.e., a fraction of a wavelength) will couple most significantly to the sea water. This coupling will affect both the impedance and radiation characteristics of the antenna elements, making it difficult to determine appropriate element weights.

In conclusion, the Counselman turnstile array performs poorly when placed above sea water because it is optimized only for the case where it is in the vertical orientation with respect to the ocean surface. Because the multipath-abating antenna will often be tilted when placed in a buoy, the turnstile array was rejected as a possible candidate design.

2.2 QHA ELEMENT

An antenna element that is better suited for the current application because it can be designed to have a radiation pattern with a large front-to-back ratio is a QHA, or volute, as shown in figure 2-4. A QHA consists of four identical helices, each spaced 90° apart and fed with voltages of equal amplitude and in time-phase quadrature. Equivalently, a QHA consists of two identical bifilar helices that are orthogonal and excited in time-phase quadrature. The QHA behaves as an interleaved endfire array with a largely hemispherical overhead, unidirectional pattern and circular polarization. As a result, this antenna is somewhat immune to reflections when located above a ground plane. In addition, a bifilar helix is a predominantly closed antenna, with its interleaved elements highly coupled to each other. This self-coupling reduces its sensitivity to the existence of nearby structures, especially those located along the helical axis. An overview of the circuit and radiation characteristics of the volute with design information has been presented in several papers by Kilgus (references 7 and 8).

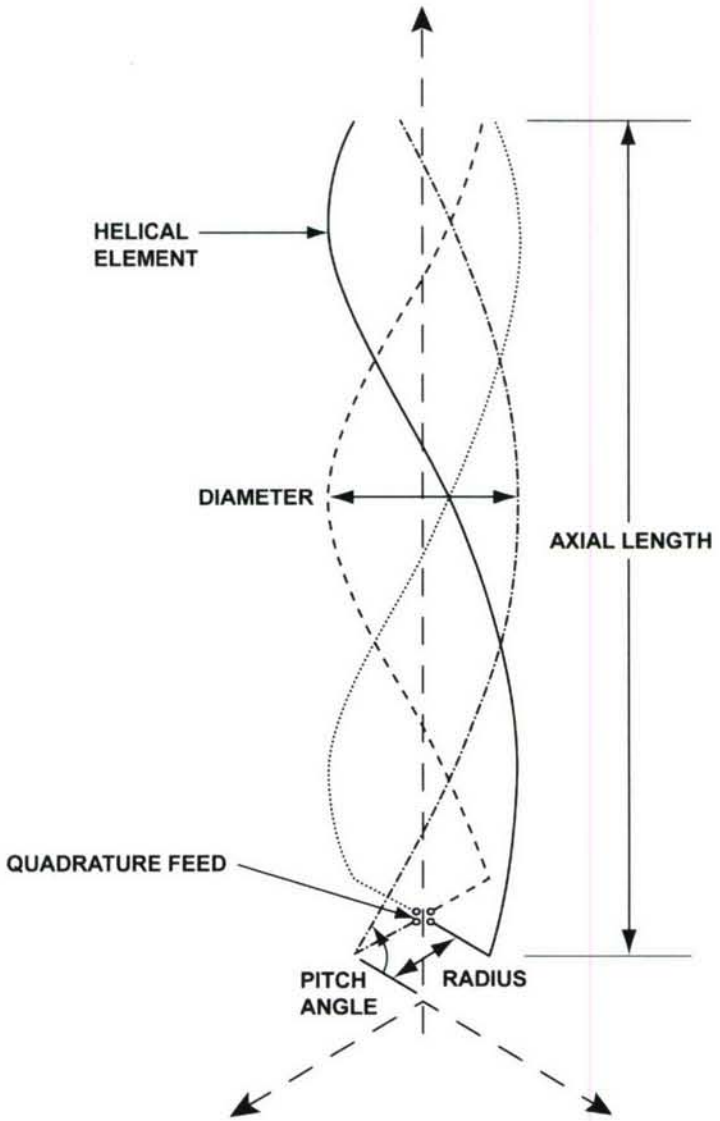

Figure 2-4. Quadrifilar Helical Antenna
(¾-turn and open-ended)

Narrow, resonant QHAs in the range of 0.1 to 0.2 λ in diameter and with element lengths of less than 1 λ possess large pattern front-to-back ratios on the order of 15 to 20 dB. As an example, consider a ¾-turn, ¾-λ long open-circuited QHA with a radius of 0.05937 λ. This antenna has a pitch angle of 66.1° and an axial length of 0.6314 λ. This QHA has a rather broad overhead pattern with an impedance bandwidth of 12.5% and a resonant impedance of approximately 100 ohms, which can be easily matched to a 50-ohm transmission line with a 180° power divider.

The narrow QHA described above was modeled (with NEC 4.1) both in free space and above a sea water half-space, at base heights h ranging from just above 0 in. to 27 in. above sea water (in 9-in. increments) and vertical tilt angles ranging from 0° to 90° (in 10° increments). Computed patterns of the total gain of the antenna in free space and at various heights above sea water at a frequency of 2.45 GHz are given in figure 2-5. The patterns show only a small amount of multipath interference that is most noticeable at low elevation angles and for large antenna heights above the sea water. Figure 2-5 shows that the maximum loss in gain (from the free-space value) due to multipath interference is approximately 4 dB and occurs when h = 27 in. (= 5.60 λ). Overall, the narrow QHA has good immunity with respect to multipath interference.

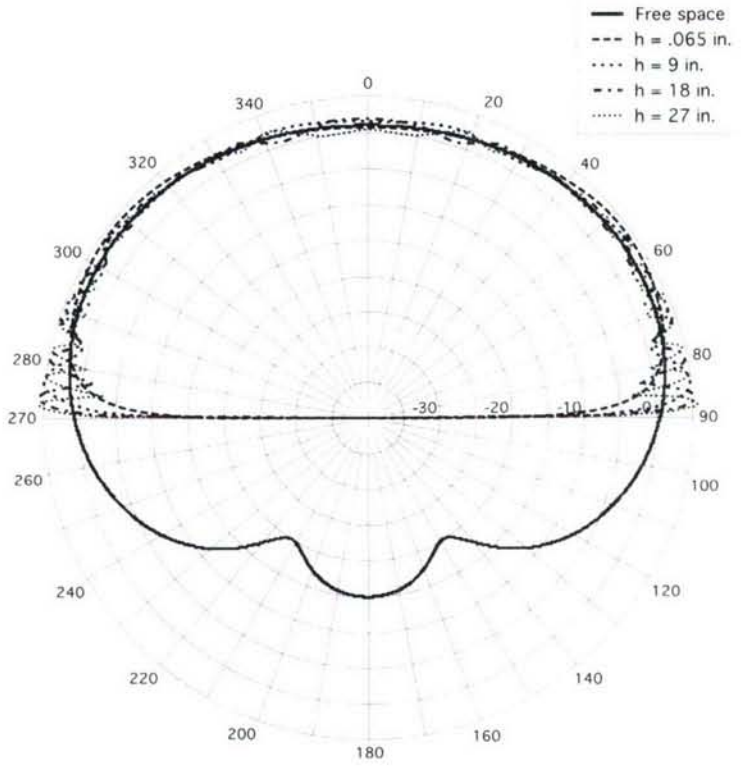

Figure 2-5. Computed Total Gain Patterns (dB) in the Vertical Plane at 2.45 GHz of a Resonant QHA (3/4 Turn, 3/4 λ Long, 0.05937 λ Radius, 66.1° Pitch Angle, 0.6314 λ Axial Length) in Free Space and at Various Base Heights Above Sea Water

Computed radiation patterns of the total gain of the narrow QHA oriented at tilt angles of 20° and 40° (with respect to the vertical) above sea water at 2.45 GHz are shown in figure 2-6. A comparison of the QHA pattern in figure 2-6a with the turnstile array pattern in figures 2-3 for the 20° tilt case indicates that the QHA element possesses much greater immunity with respect to multipath interference than the turnstile array. It should be noted that the turnstile array patterns in figure 2-3 were computed at a lower frequency (1.57542 GHz) than the operating frequency (2.45 GHz) used in the evaluation of the QHA patterns in figure 2-6. Therefore, the heights above sea water plotted in figure 2-3 are actually electrically shorter than the corresponding heights plotted in figure 2-6. In particular, $h = 18$ in. in figure 2-3 is equivalent to $h/\lambda = 2.4$, and $h = 18$ in. and $h = 27$ in. in figure 2-6 are equivalent to $h/\lambda = 3.73$ and $h/\lambda = 5.60$, respectively. Consequently, the patterns of the tilted turnstile array in figure 2-3 would have to be raised to greater heights above sea water to be compared with the QHA patterns in figure 2-6a, resulting in additional multipath interference in the turnstile array. A comparison of figures 2-6a and 2-6b indicates that as the tilt angle of the QHA is increased from 20° to 40°, only a small amount of additional multipath interference results. Therefore, the radiation field of the narrow QHA should have good immunity with respect to multipath interference when placed above a dynamic sea surface.

The above results show that one narrow QHA has superior pattern performance above a dynamic sea surface than Counselman's five-element turnstile array. It is anticipated that an array of QHAs will provide both the gain requirements and the necessary pattern immunity with respect to multipath interference when located above sea water. Therefore, the QHA appears to be a more suitable antenna element for this application.

(a)

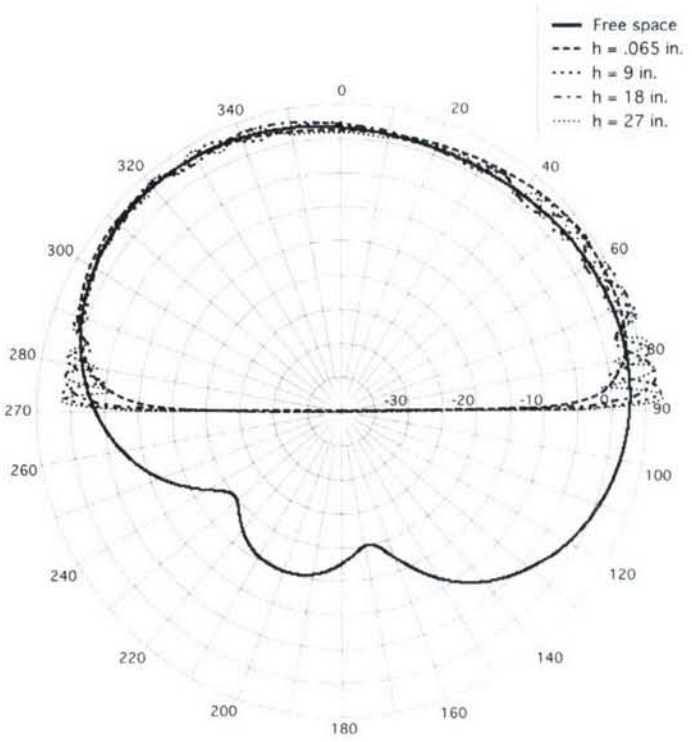

(b)

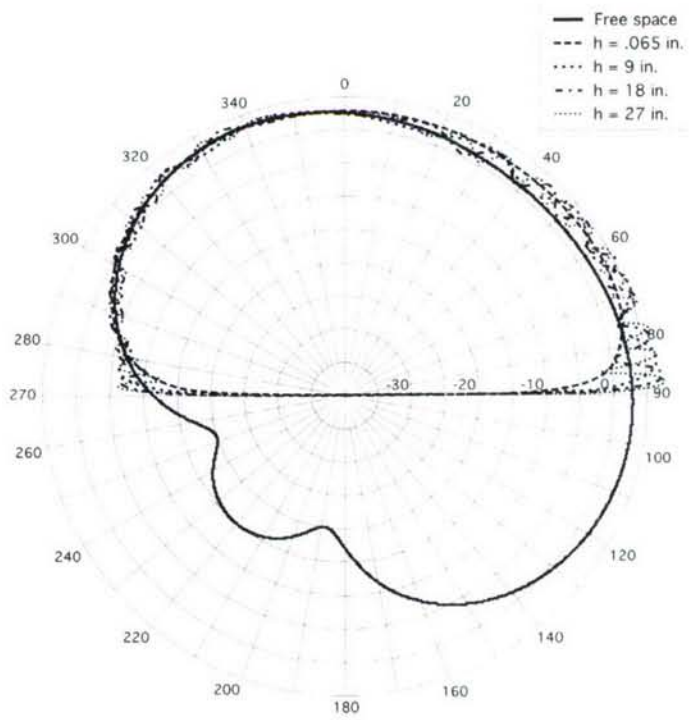

Figure 2-6. Computed Gain Patterns (dB) in the Vertical Plane at 2.45 GHz of the Resonant QHA Described in Figure 2-4 and Tilted with Respect to the Vertical Position in Free Space and at Various Base Heights Above Sea Water: (a) Tilt Angle = 20° and (b) Tilt Angle = 40°

In addition to the radiation pattern performance of an antenna element in the presence of a dynamic sea surface, it is also important to consider the impedance properties of the antenna under these conditions. In particular, the antenna should not couple (electromagnetically) to the sea surface such that its impedance varies with time under various sea-state conditions. Equivalently, the input impedance of each antenna element should be independent of tilt angle over the range of buoy motion that is anticipated. If the element impedances vary significantly with orientation above the ocean surface, the array will experience losses due to impedance mismatch and will create additional challenges in the beamformer design. Therefore, it is important that each array element has stable impedance characteristics in a dynamic ocean environment.

To evaluate the effect of tilt angle on the input impedance of the $\frac{3}{4}$-λ long QHA described in figure 2-5, consider a thin-wire model of the antenna above a 36-in. diameter circular ground plane illustrated in figure 2-7. The ground plane, modeled as a wire mesh, extends across the top surface of the buoy. The ground plane was added to the model to provide a more stable reflecting surface, at least for higher elevation angles of incidence, resulting in possibly more stable impedance characteristics. Although the ground plane was included in this preliminary analysis, it was later found to be unnecessary and was eliminated. In the analysis described below, the ground plane is placed at 9 in. above sea water (corresponding to the nominal height of the top surface of the buoy above the sea water) and the axial height h from the base of the helix to the circular ground plane is varied. In addition, the QHA and ground plane were tilted from the upright vertical position for angles ranging from 0 to 40°. All calculations were performed at 2.45 GHz using NEC.

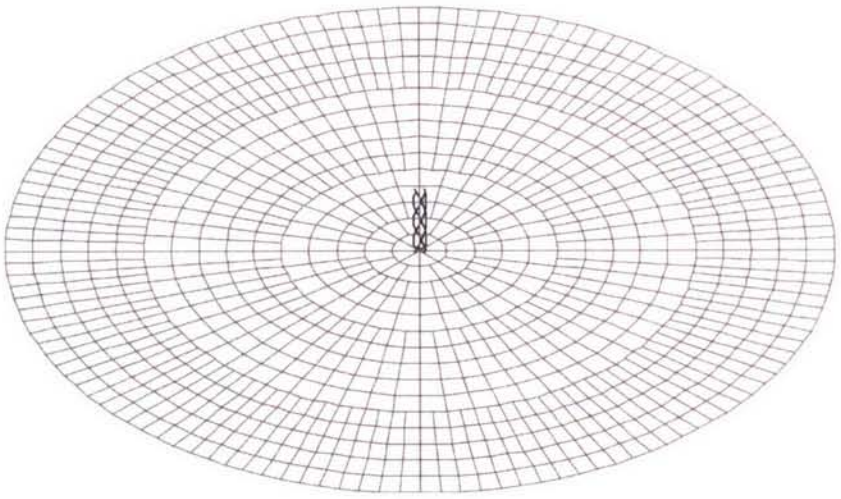

Figure 2-7. Thin-Wire Model of the Resonant QHA Described in Figure 2-5 Above a 36-in. Diameter Circular Ground Plane

Figures 2-8a and 2-8b show plots of the input resistance and reactance, respectively, of one feed of the QHA as a function of tilt angle for various antenna base heights h above the circular ground plane. The plots show that the impedance is sensitive to tilt angle only when it is close to the ground plane. At a 6-in. height ($h = 1.24\ \lambda$) above the ground plane, only the input reactance shows a slight variation with tilt angle. For heights of 12 in. or greater above the ground plane (i.e., $h \geq 2.49\ \lambda$), the impedance shows little variation. Therefore, in the design of a linear array of QHAs, the bottom element should be placed at least 1 - 2 λ above the ground plane to have negligible coupling to the sea water. Note that this analysis ignores the effect of element mutual coupling in the array.

(a)

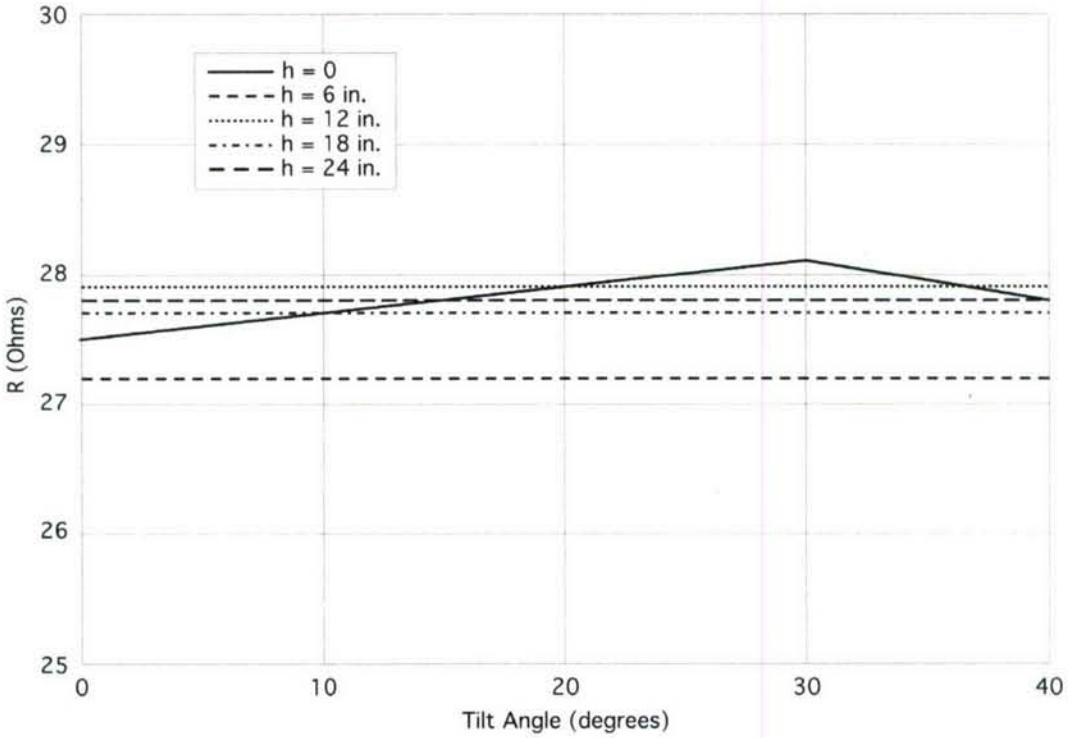

(b)

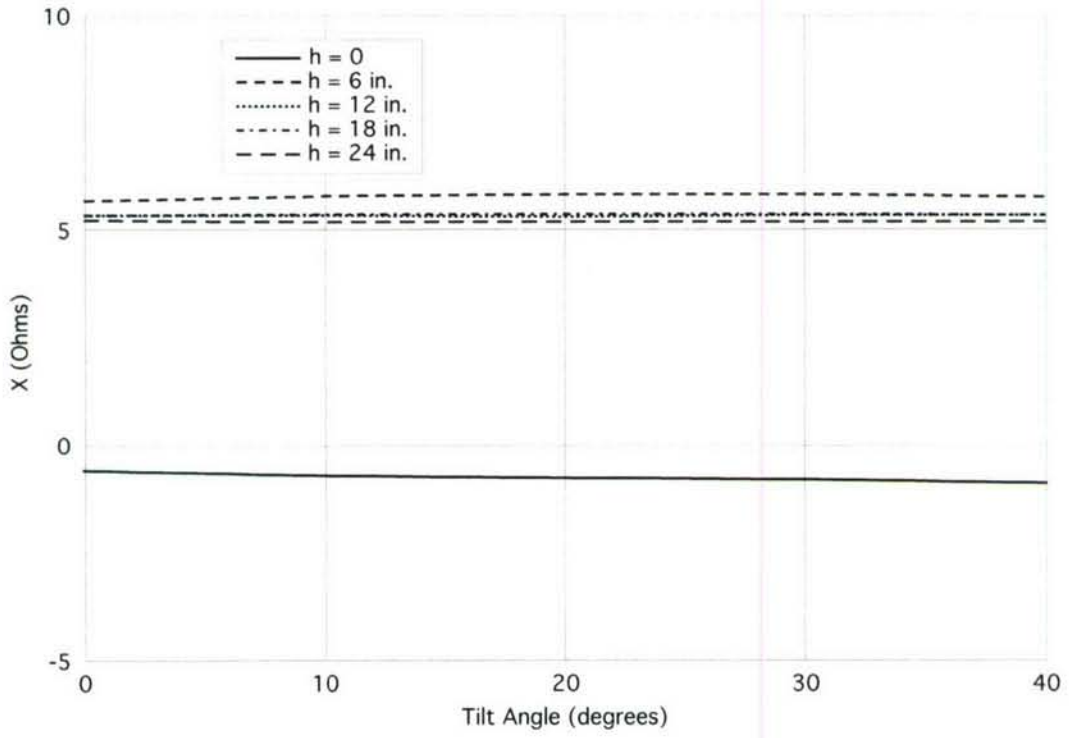

Figure 2-8. Input Impedance of One Feed Arm of the QHA Described in Figure 2-5 at 2.45 GHz as a Function of Tilt Angle for Various Base Heights Above a 36-in. Diameter Circular Ground Plane: (a) Resistance and (b) Reactance

3. DETERMINATION OF OPTIMUM QHA ELEMENT DESIGN PARAMETERS

In the design of a linear array consisting of four QHA elements, 16 coaxial cables are required to feed the array. It was determined that the feed cables must fit within the interior of the array and travel along a direction parallel to the helical axis before connecting to the appropriate helical element. In addition, the feed cables must fit within a metallic tube or conduit to shield the cables from the radiating elements. Despite its desirable properties that include a radiation pattern with a large front-to-back ratio, wide beamwidth, and an acceptable bandwidth and matchable input impedance, the diameter (0.119 λ) of the $\frac{3}{4}$-turn, $\frac{3}{4}$-λ long open-circuited QHA studied in the previous section was found to be too narrow to allow passage of the 16 feed cables.

To maintain the geometrical symmetry of each QHA element, the axis of the metallic tube must be coincident with the array axis. The tube diameter must be made as small as possible to maintain a symmetrical arrangement of feed cables and QHA arms. A large tube diameter will degrade the element radiation patterns by increasing the radiation along the backside direction. In addition, a large tube diameter will decrease the impedance bandwidth of the QHA. Therefore, the metallic feed tube must be made as narrow as possible to preserve the desirable circuit and radiation characteristics observed for the QHA in the previous section.

A large-diameter QHA generally has a wider impedance bandwidth than a narrow QHA. A QHA with a pitch angle less than 50° and a total element length of at least about 1.5 λ operates above the "cut-in" frequency when the axial length per turn is approximately 0.5 λ. This cut-in frequency is defined as the frequency above which the QHA impedance has little variation and becomes mainly resistive; resulting in a low voltage standing wave ratio (VSWR) and, therefore, the QHA operates as a wide-bandwidth antenna. Note that a cut-in frequency does not exist for all QHA designs; therefore, a QHA operating above the cut-in frequency does not have to operate at resistive resonance to match its impedance. The following are some disadvantages of a large-diameter QHA:

1. A QHA with a diameter greater than 0.2 λ tends to produce more backside radiation that is attributed to the increased radiation from its wider radial feed sections.

2. Although a QHA produces minimum backside radiation at the cut-in frequency, the backside radiation increases with frequency above the cut-in value.

3. The larger radial feed sections associated with a large-diameter QHA will tend to couple more to the sea water below it.

It should be noted that the axial length per turn of a QHA at which point the cut-in frequency occurs is dependent on the helical pitch angle. Figure 3-1 is a plot of the computed axial length per turn as a function of pitch angle where the cut-in frequency occurs. The plot was produced from a NEC model (reference 5) of the QHA. The plot shows that at a pitch angle of 40° the cut-in frequency occurs at an axial length per turn of 0.5 λ.

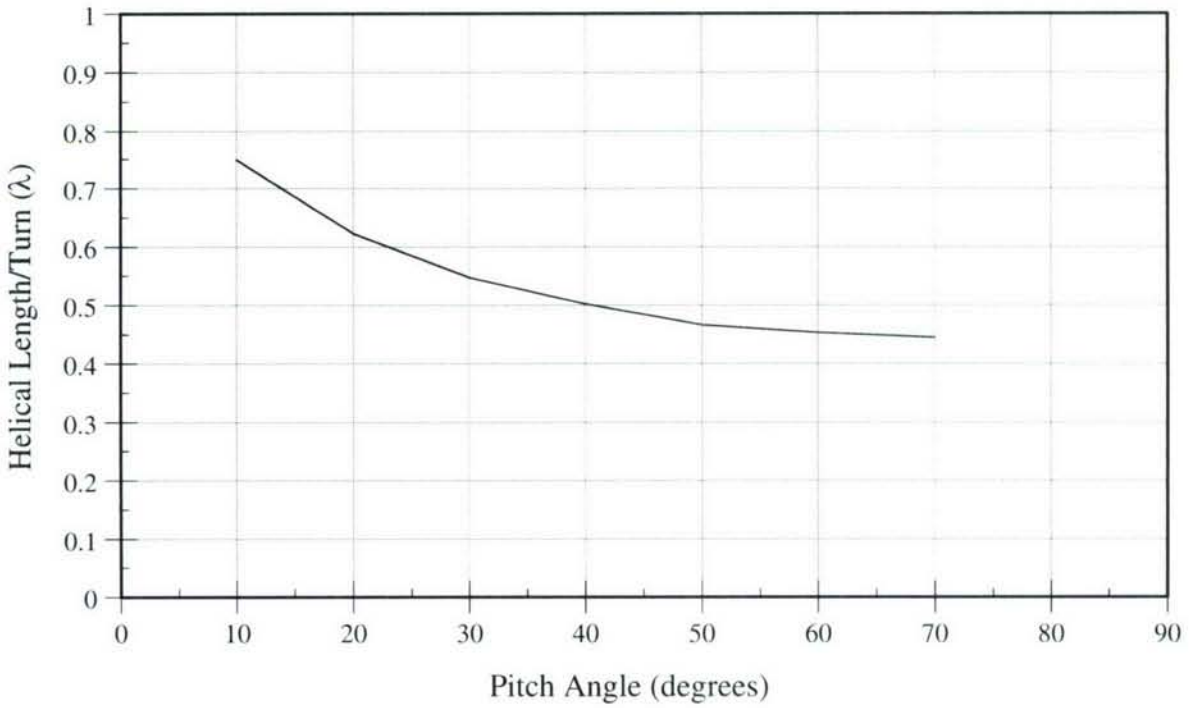

Figure 3-1. Computed Helical Length per Turn (in Wavelengths) as a Function of Pitch Angle of a QHA Where Cut-In Occurs

A parametric study was performed to determine the optimum design parameters for the QHA element. The investigation was carried out with a thin-wire model of a forward-fire, open-circuited QHA via the NEC code. The QHA parameters that were varied were the helical radius, element length, and pitch angle. Initially, the axial length of the QHA was varied rather than the helical element length because of the spacing requirements between the array elements. However, because the radiation patterns are largely governed by element length, the parametric runs were performed using element length as a variable instead of the axial length. The axial length of the QHA was monitored by visual inspection of the model where necessary. In the parametric investigation, the circumference was varied from 0.1 λ to 1.0 λ in increments of 0.1 λ (equivalent to varying the helical radius from 0.0159 λ to 0.159 λ in increments of 0.0159 λ), the helical element length was varied from 0.125 λ to 2.0 λ in increments of 0.125 λ, and the pitch angle was varied from 10° to 90° in increments of 10°. In all, a total of 1440 antennas were modeled.

In the parametric study, the pattern beamwidth and front-to-back ratio were used to determine the optimum QHA element design for the array. Acceptable pattern front-to-back ratios, on the order of 12 – 17 dB, were found to correspond to QHA designs with pitch angles between 30° and 50°, a helical element length of 1.25 – 1.5 λ, and a helical radius of 0.125 λ. Table 3-1 lists four QHA designs that fell within these ranges. Note that the helical radii listed in table 3-1 are approximately double the size of the QHA investigated in section 2.

Table 3-1. Optimum Design Parameters of QHA Element Obtained from Thin-Wire Model Analysis

Element Length (λ)	Pitch Angle (deg.)	Helix Radius (λ)	Helix Radius (in.)	Axial Length (λ)	Axial Length (in.)	Pattern Front-to-Back Ratio (dB)
1.25	30	0.127	0.612	0.562	2.71	15.0
1.25	40	0.127	0.612	0.721	3.48	12.5
1.50	30	0.112	0.540	0.694	3.35	17.5
1.50	40	0.112	0.540	0.892	4.38	17.5

Caution must be taken in using the pattern front-to-back ratio as the sole parameter for determining the optimum QHA design because only the overhead and backside (i.e., axial) gains

are involved. Therefore, the patterns of the total gain in free space should be studied for each case. For example, a QHA with a 60° pitch angle and helical radius of 0.112 λ has a pattern front-to-back ratio of 19 dB, but the main overhead beam is split into two beams and, therefore, will not provide suitable hemispherical coverage. It was found that to radiate a single overhead beam, the QHA must have a pitch angle of 40° or less.

The computed free-space radiation patterns and Smith charts of the input impedance for each of the QHA designs listed in table 3-1 are shown in figures 3-2 to 3-5. A comparison of the total gain patterns shows that figures 3-3a and 3-5a exhibit a wider beamwidth than those in figures 3-2a and 3-4a. This is a desirable feature and results from the antennas having a larger pitch angle. However, as indicated in table 3-1, because the axial length of the QHA increases with pitch angle, the spacing between array elements must also increase. Too large of an element spacing will result in the appearance of grating lobes in the array radiation pattern. Consequently, to eliminate the existence of grating lobes in the radiation pattern of the array, an upper limit must be imposed on the pitch angle to keep the spacing between elements sufficiently small. The maximum allowable spacing between array elements was set at ⅞ λ.

The normalized impedance loci for each QHA design in table 3-1 are illustrated in figures 3-2b to 3-5b. In these Smith charts, the impedances are normalized by 100 ohms. The impedance plotted corresponds to that across two helical arms, or equivalently, one bifilar pair of the QHA. The impedance plots show that the characteristic impedance Z_0 of each QHA is approximately 300 ohms. The characteristic impedance of a QHA is the resistance that the impedance locus approaches as the frequency increases toward infinity, or equivalently, is the resistance that the impedance approaches above the cut-in frequency. Because the QHAs were modeled in NEC with thin-wire helical elements, the characteristic impedance depends primarily on the wire diameter, and to a lesser extent, the pitch angle (note that $Z_0 = \frac{3}{2}\sqrt{\frac{L}{C}}$, where L is the inductance per unit length of helical element and C is the capacitance per unit length between the two helical elements of a bifilar helix).

(a)

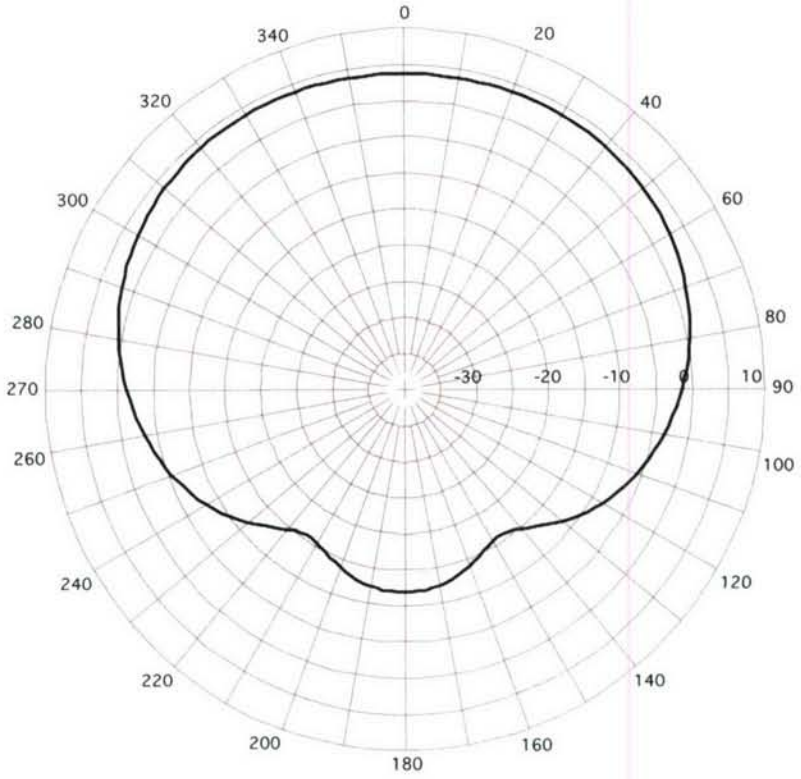

(b)

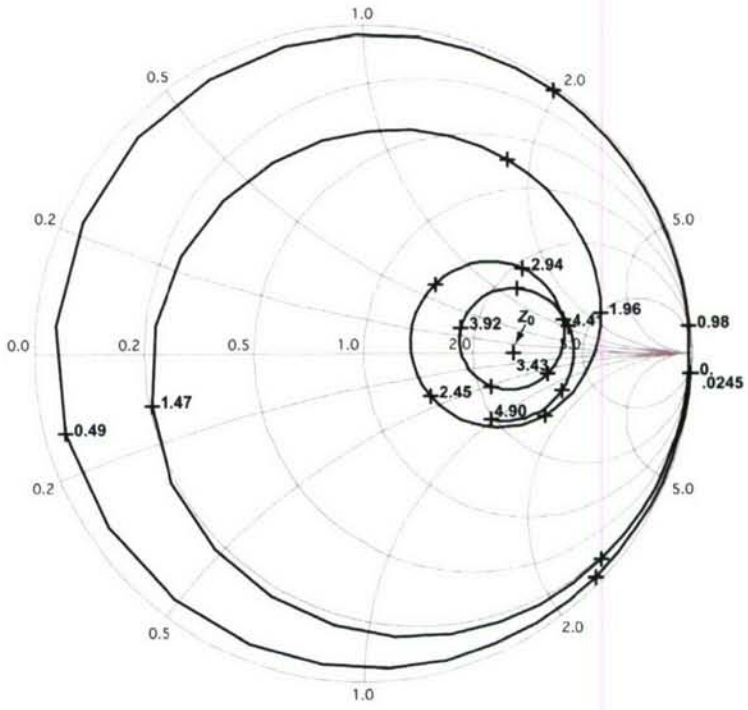

Figure 3-2. QHA (Element Length = 1.25 λ, Radius = 0.127 λ, Pitch Angle = 30°, Axial Length = 0.562 λ) in Free Space: (a) Computed Directive Gain Pattern (dB) at 2.45 GHz and (b) Smith Chart of the Computed Input Impedance of One Bifilar Pair

(a)

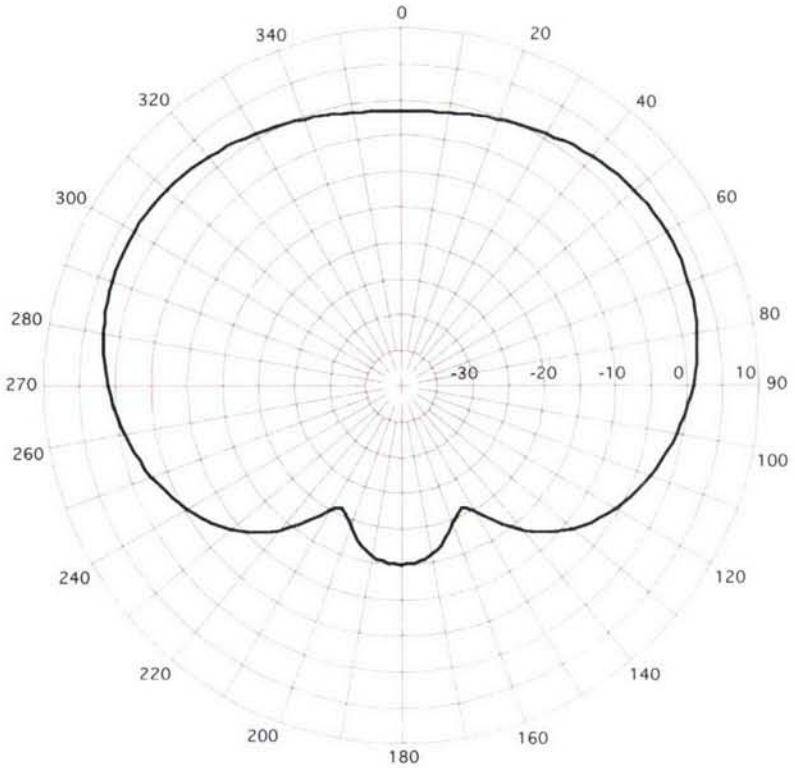

(b)

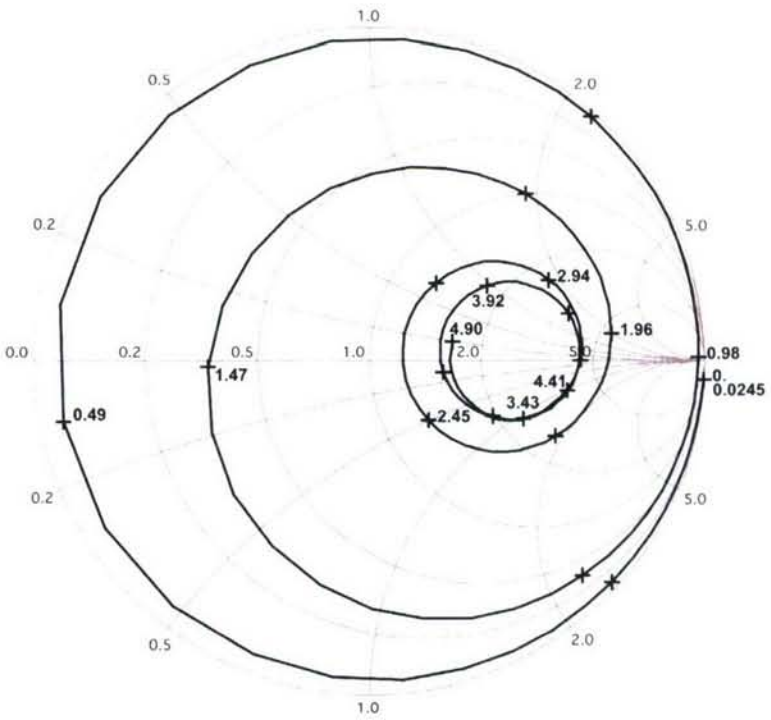

Figure 3-3. QHA (Element Length = 1.25 λ, Radius = 0.127 λ, Pitch Angle = 40°, Axial Length = 0.721 λ) in Free Space: (a) Computed Directive Gain Pattern (dB) at 2.45 GHz and (b) Smith Chart of the Computed Input Impedance of One Bifilar Pair

(a)

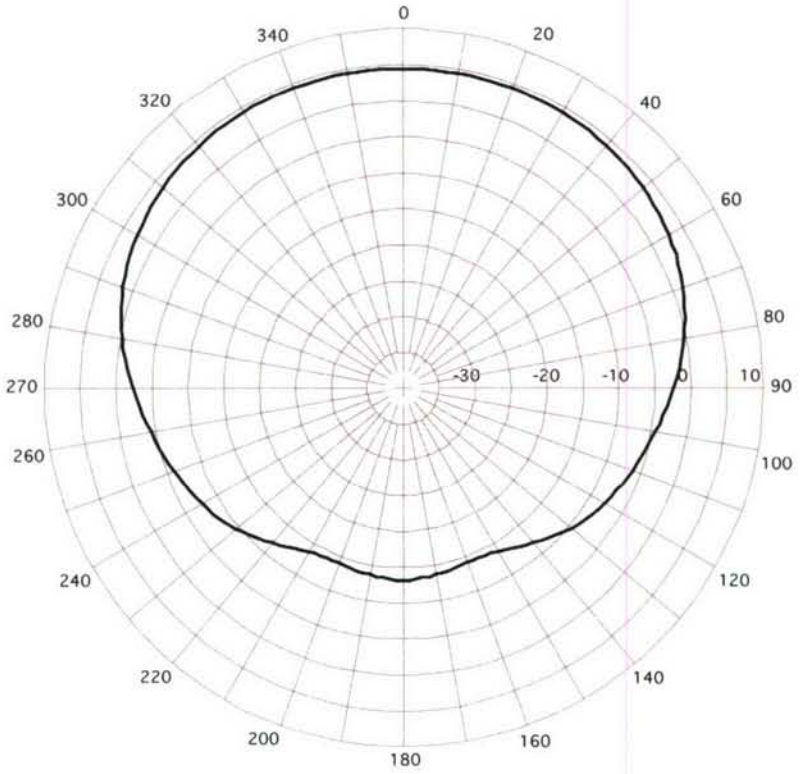

(b)

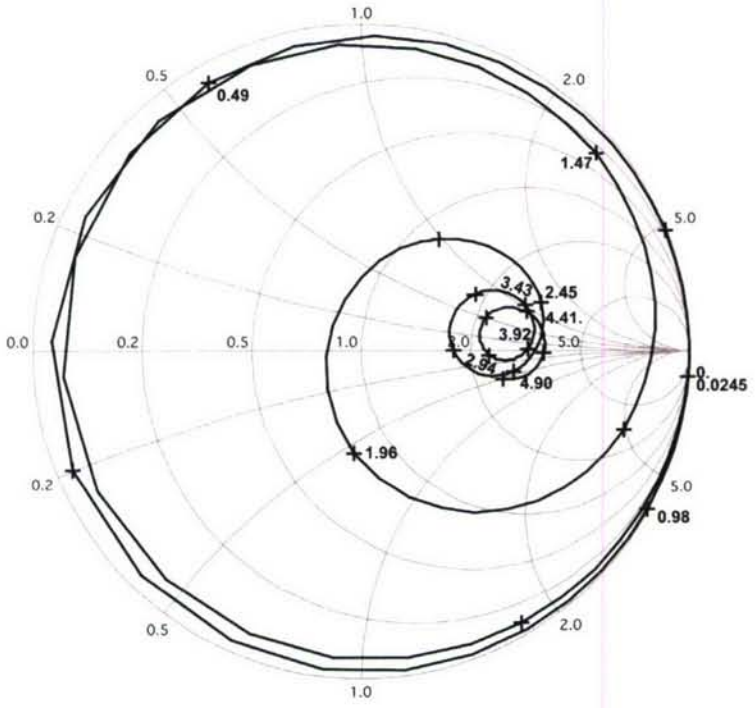

Figure 3-4. QHA (Element Length = 1.5 λ, Radius = 0.112 λ, Pitch Angle = 30°, Axial Length = 0. 694 λ) in Free Space: (a) Computed Directive Gain Pattern (dB) at 2.45 GHz and (b) Smith Chart of the Computed Input Impedance of One Bifilar Pair

(a)

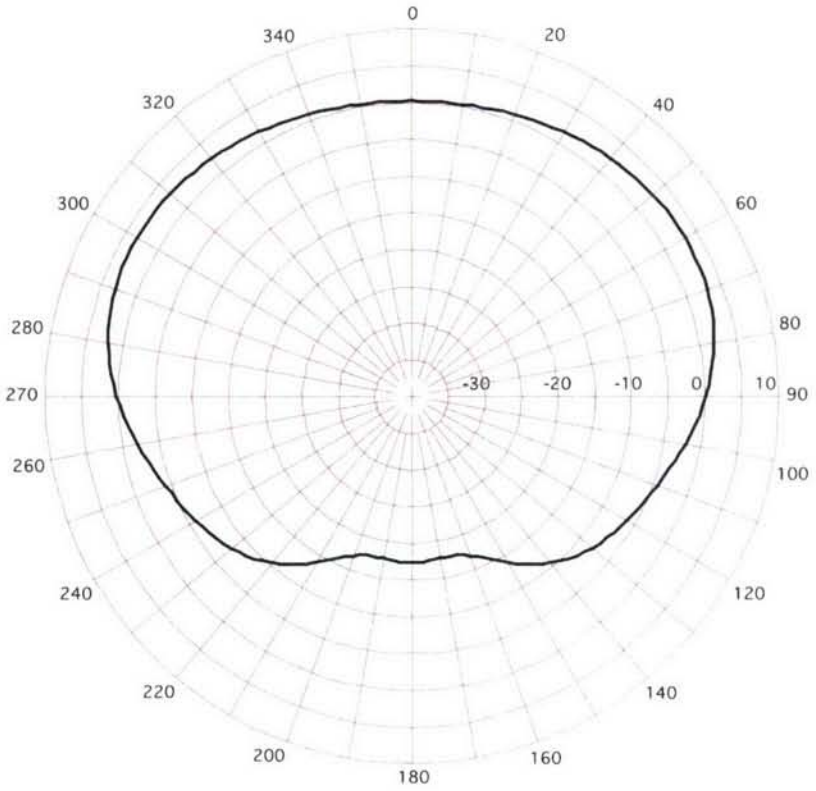

(b)

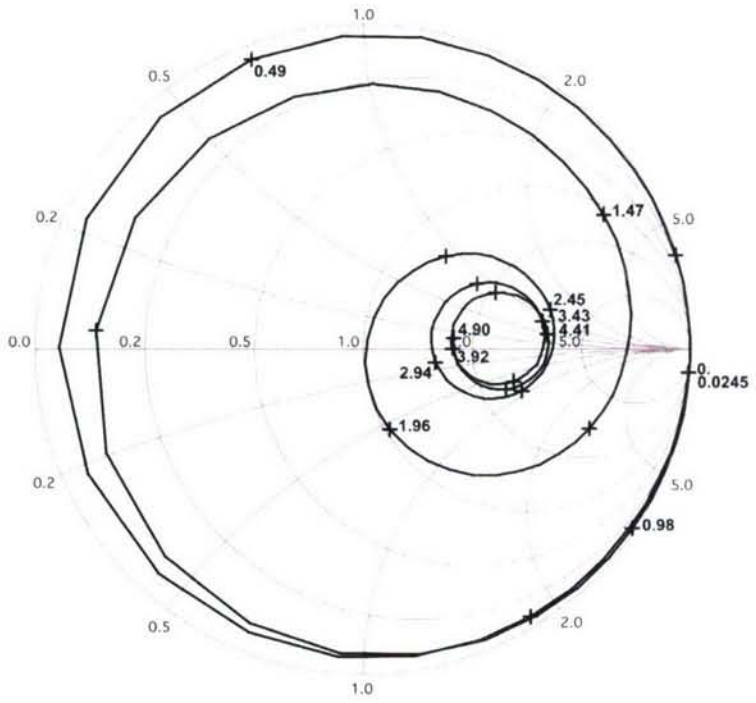

Figure 3-5. QHA (Element Length = 1.5 λ, Radius = 0.112 λ, Pitch Angle = 40°, Axial Length = 0.892 λ) in Free Space: (a) Computed Directive Gain Pattern (dB) at 2.45 GHz and (b) Smith Chart of the Computed Input Impedance of One Bifilar Pair

Thin wires have large L and small C and, thus, Z_0 is large. Wide elements have small L and large C, and thus Z_0 is small. If the helical wires are replaced with wide strip elements (that comprise a large percentage of the available surface area), Z_0 can reduce to approximately 100 ohms, thus allowing the QHA to be easily matched to a 180° power splitter. Strip helical elements of sufficient width will tend to improve the convergence of the impedance locus about Z_0 over that of the thin helical wires in the NEC model due to wider elements with less inductance and a little more bandwidth. It is also anticipated that the introduction of a metal tube placed along the QHA axis that contains the feed cables will produce a small change in the impedance (i.e., a decrease in Z_0 because the capacitance per unit length of element increases) and a minor reduction in impedance bandwidth.

To avoid the occurrence of grating lobes in the array radiation pattern and allow for a QHA element of sufficiently long axial length, the element separation was set to 0.75 λ, equivalent to 3.61 in. at 2.45 GHz. This separation permits a QHA element design with a sufficiently wide impedance bandwidth and a free-space radiation pattern with only a small amount of backside radiation. In addition, sufficient spacing between array elements must be included to reduce the interelement mutual coupling. These constraints resulted in the selection of a QHA element design with the parameters listed in table 3-2. The radiation pattern and normalized impedance locus of the selected element design in free space are illustrated in figures 3-2a and 3-2b, respectively.

Table 3-2. Parameters of Selected QHA Element Design

Parameter	Value
Pitch Angle	30°
Total Element Length	6.03 in. (1.25 λ)
Axial Length	2.71 in. (0.562 λ)
Helical Radius	0.612 in. (0.127 λ)

A QHA element with the design parameters given above was constructed and measured to experimentally verify the circuit and radiation characteristics that were predicted by the NEC model. Figure 3-6 shows photos of the antenna and associated feed network. The helical conductors each consist of 3-mil-thick copper tape of width 0.866 in. that is bonded to a 3-mil-thick Mylar sheet. The edges of the copper tape were cut by placing the copper-covered sheet into a mechanical plotter and using a diamond scribe to cut the edges.

(a)

(b)

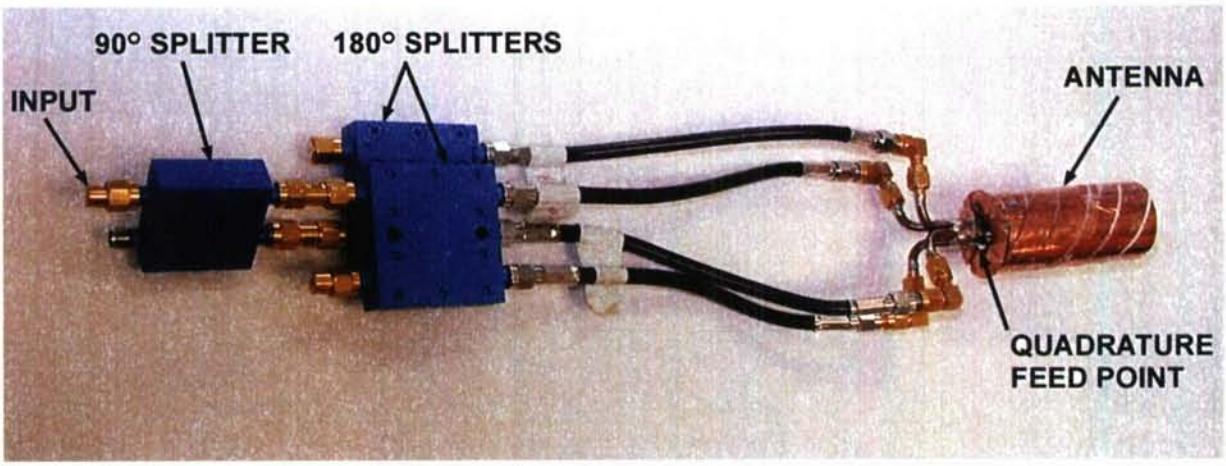

Figure 3-6. Constructed QHA:
(a) Closeup View of Antenna and (b) Antenna Connected to Feed Network

The quadrature feed point for the antenna was made by soldering together the outer conductors of a square bundle of four 0.141-in. outer diameter semirigid cables, and the center conductors became the feeds for the four helical elements. Because the center conductors of the feed cables were physically displaced from each other, the QHA was not fed from a single point, but instead from points slightly displaced (radially) from the axis, as shown in figure 3-6. (As will be shown in the following section, the concept of "radially displaced feed points" occurred once the metal tube was inserted along the axis of the QHA array. For the constructed QHA in figure 3-6, the feed points are only slightly displaced from the QHA axis, resulting in small changes in its impedance. Once the tube is inserted, the displacement of the feed points becomes much larger with more noticeable changes in the impedance.) As a result, it was anticipated that the measured impedances would not exactly match those predicted in figure 3-2b.

The impedance plot in figure 3-2b is based on a NEC model of the selected QHA element design with thin-wire conducting elements. In contrast, the constructed antenna in figure 3-6 has wide strip conductors and, therefore, has a smaller measured impedance than that computed in figure 3-2b. The desired characteristic impedance Z_0 of the QHA element is 100 ohms as compared with the predicted value of 300 ohms in the NEC model. Although the thin-wire model of the QHA predicted much higher impedances than that of the constructed QHA with wide strip conducting elements, the computed VSWR should be close to the measured VSWR. In addition, a QHA with thin-wire conductors will produce less backside radiation than a QHA with thick conductors. The QHA shown in figure 3-6 was constructed with wide strips to obtain a characteristic impedance at the target value of 100 ohms.

The construction of the antenna required lining up the radial sections of the helical elements (etched on a Mylar sheet) to the corresponding circumferential sections and soldering the boundary between each of them. This process can lead to physical asymmetries between the elements producing asymmetries in the radiation pattern, some of which may be seen in the measured patterns.

The helical conductors ideally occupy 97.5% of the available surface area along the helical circumference in order to produce an impedance across each bifilar helical pair that is close to

100 ohms. Because of construction limitations in the attempt to create small slots between the conducting elements, the amount of available surface area occupied by the helical conductors was reduced to 90%, resulting in a small increase in the characteristic impedance. It should be recalled that a QHA consists of two orthogonal bifilar helices that are fed 90° out of phase. The feed network in figure 3-6b provides a quadrature feed for the antenna. The four coaxial cables at the bottom of the antenna are connected to the output of a pair of 180° power splitters that are in turn connected to the output of a 90° power splitter. In the receive mode, the signal power from the antenna appears at the input to the 90° power splitter.

Figure 3-7a shows plots of the measured gain as a function of elevation angle at 2.45 GHz for the QHA in figure 3-6. The gain pattern plots are shown for vertical, horizontal, and right-hand circular polarizations. The measured gain patterns show some asymmetry that is attributed to asymmetries in the feed network and in the mechanical construction of the antenna. These asymmetries are not observed in the computed patterns shown in figure 3-2a. Note that figure 3-2a is a plot of the total antenna gain, which is a combination of both the vertical and horizontal polarizations. From figure 3-7a, the measured pattern front-to-back ratio of the QHA is approximately 10 dB as compared with the computed value of 15 dB observed in figure 3-2a. The 5-dB reduction in the measured pattern front-to-back ratio is attributed to the increased backside radiation caused by the antenna asymmetries and by the use of the wide helical conducting elements.

Figure 3-7b shows plots of the measured VSWR of both bifilar feeds of the constructed QHA in figure 3-6 as a function of frequency. It should be noted that the impedance (that produced the VSWR plot in figure 3-7b) was measured through one 180° power splitter and a short length of cable connecting the power splitter to the antenna. The short length of cable has a small loss; thus, the measured VSWR is slightly lower than that of the antenna. In addition, the power splitters are designed to operate from 2 to 4 GHz; thus, the measured impedances outside of this range will probably have some error. The plots show a low VSWR of magnitude less than 2.3 for frequencies above 2.2 GHz.

(a)

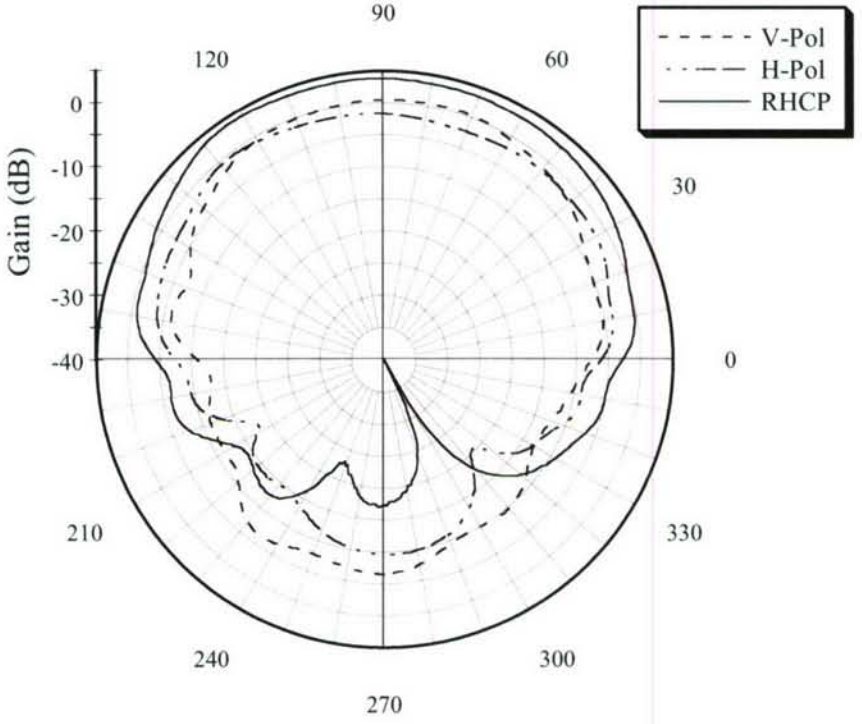

(b)

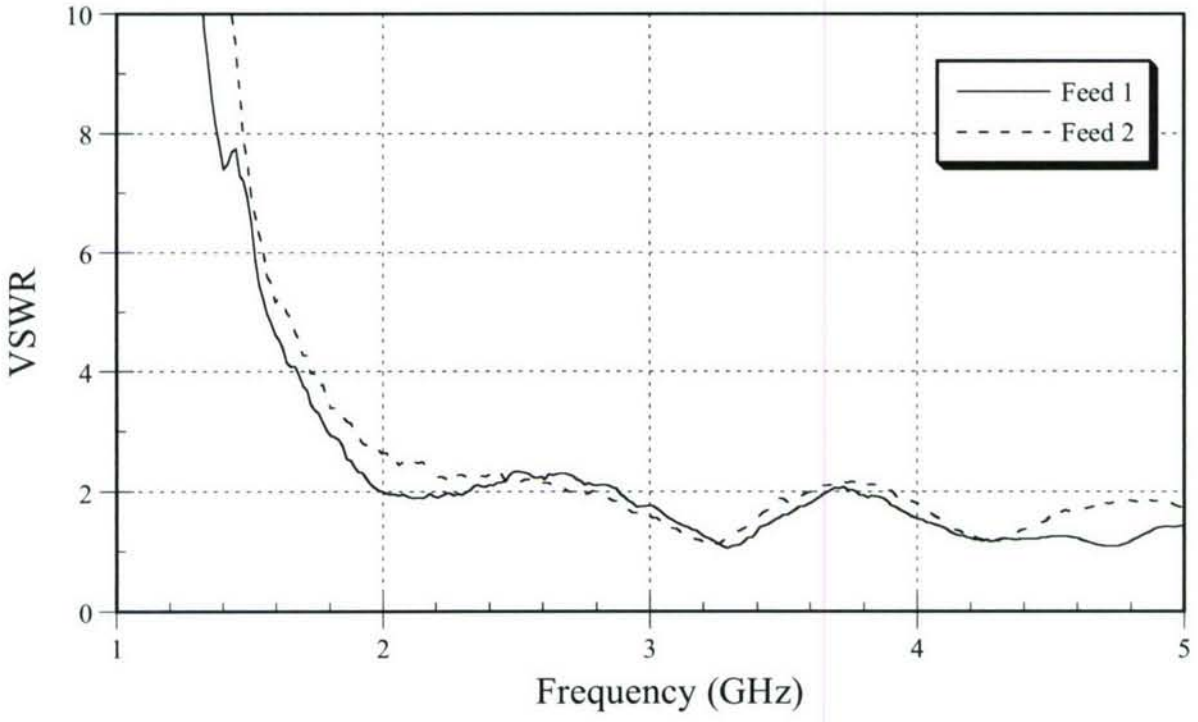

Figure 3-7. Measured Circuit and Radiation Characteristics of the Constructed QHA Shown in Figure 3-6: (a) Gain Patterns at 2.45 GHz and (b) Input VSWR of Both Feed Arms

Figure 3-8 shows Smith charts of the measured impedance loci for both bifilar feeds of the constructed QHA. The plots of the measured impedance show that above the cut-in frequency the impedance locus spirals inward toward a characteristic impedance Z_0 of magnitude slightly above 100 ohms and rotated in the inductive direction. In comparison, the computed characteristic impedance obtained from figure 3-2b has a larger magnitude than the measured values because of the narrow, thin-wire helical elements used in the model. The measured inductive component of Z_0 may be attributed to two possible sources: (1) the slightly displaced feed point attributed to the separation of the feed-cable center conductors from the antenna axis, and (2) the short length of center conductor required to connect the cables to the radial feed sections of the helical elements. The measured impedance loci in figure 3-8 are tighter than the computed locus in figure 3-2b because the narrow conducting elements used in the model have less bandwidth than the wide-conducting strip elements used in the constructed QHA, and there is some small loss in the short cables that connect a bifilar helical section to a 180° power splitter.

In conclusion, the constructed QHA in figure 3-6 produces an acceptable radiation pattern. The VSWR of the constructed QHA at 2.45 GHz is a little high because the antenna is operating just above cut-in as can be seen from the Smith charts in figure 3-8. The impedance loci in figure 3-8 are not tightly wrapped about Z_0 in the vicinity of 2.45 GHz. To improve the impedance match of the QHA to the power splitter, the input impedance can be increased by decreasing the helical conductor width. This adjustment in the conductor width can be made to increase the characteristic impedance Z_0 to approximately 200 ohms in order that the input impedance at 2.45 GHz is approximately $Z_0/2$ or 100 ohms.

(a)

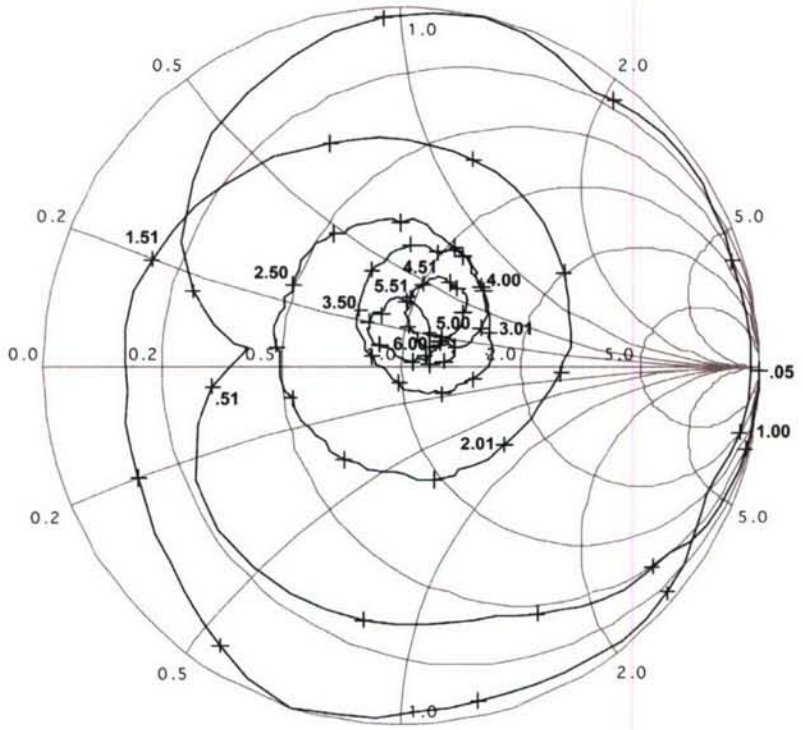

(b)

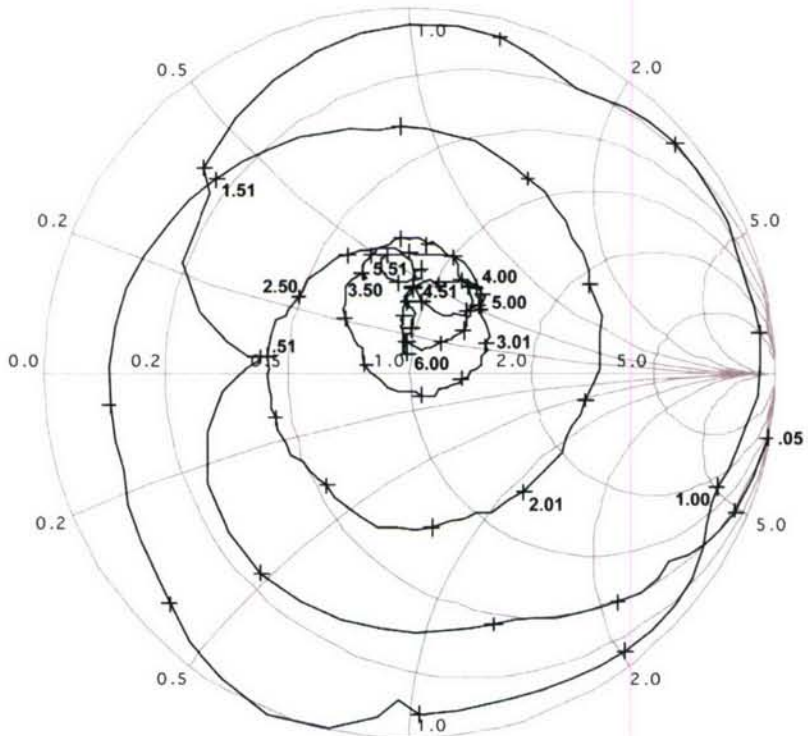

Figure 3-8. Smith Charts of the Measured Input Impedances of Both Bifilar Pairs of the Constructed QHA Shown in Figure 3-6: (a) Feed 1 and (b) Feed 2

4. QHA ARRAY DESIGN AND CONSTRUCTION

The analysis described in section 3 concluded that the array element with the optimum radiation performance that meets the size constraints for mounting on a buoy is a forward-fed, open-circuited QHA with a helical diameter of 1.224 in., a 30° pitch angle, an axial length of 2.71 in., and a helical conductor length of approximately 1.25 λ (6.03 in.) at the center frequency of 2.45 GHz. To simplify the construction of the antenna, each helical element was fed at its circumference instead of its center, thereby removing the radial sections of conductor. Consequently, the axial length of the antenna was increased from 2.71 in. to 2.90 in. to maintain the same helical element length and, thus, maintain an optimum impedance match at 2.45 GHz. Four of these QHAs were arranged as a vertically-oriented linear array with an element spacing of 3.61 in., equivalent to 0.75 λ at 2.45 GHz. This spacing was sufficiently small to remove the possibility of grating lobes and large enough to reduce significant element mutual coupling. Figure 4-1a gives an illustration of the QHA array installed on a buoy and figure 4-1b shows the dimensions of the array elements with their locations relative to the buoy surface and air-sea water interface. This section describes the mechanical construction of the element and array designs, including the feed assembly. The measured circuit and radiation characteristics of the array are deferred until the following section.

Figure 4-2 shows a vertical-plane view of the array feed-cable assembly. Each QHA element is fed by four coaxial cables, resulting in a total of 16 cables that are required to feed the entire four-element array. The feed cables travel parallel to the array axis and are enclosed in a brass tube placed interior to the QHA elements and coaxial with the array. The brass tube provides electromagnetic shielding of the feed cables from the radiating elements. The brass tube extends a short distance beyond the top and bottom array elements in order that these antennas experience approximately the same amount of coupling to the tube as the two interior elements. Each coaxial cable passes through a hole in the brass tube in order to feed a helical conductor of a QHA element. These holes are drilled at a 40° angle with respect to the vertical direction to allow for a more gradual bend of the feed cables and minimize the possibility of breaking the thin center conductor of the cable. The outer conductors of the coaxial feed cables are soldered to a brass ring that is attached to the brass tube. A cross-sectional view of the feed points of the bottom QHA element is shown in figure 4-3.

(a)

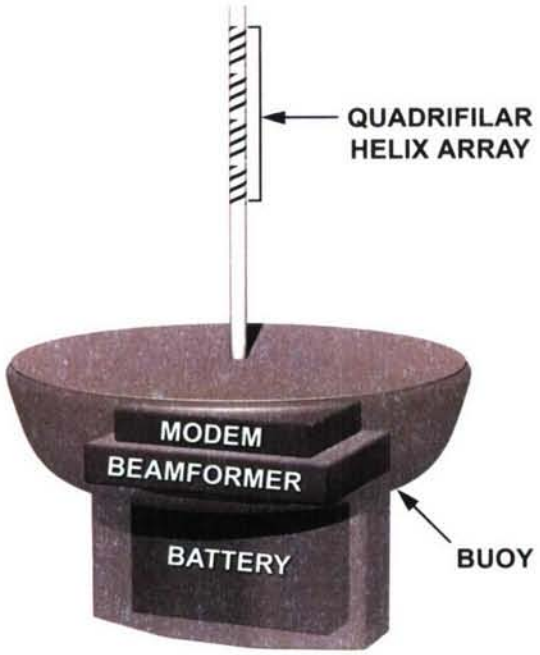

(b)

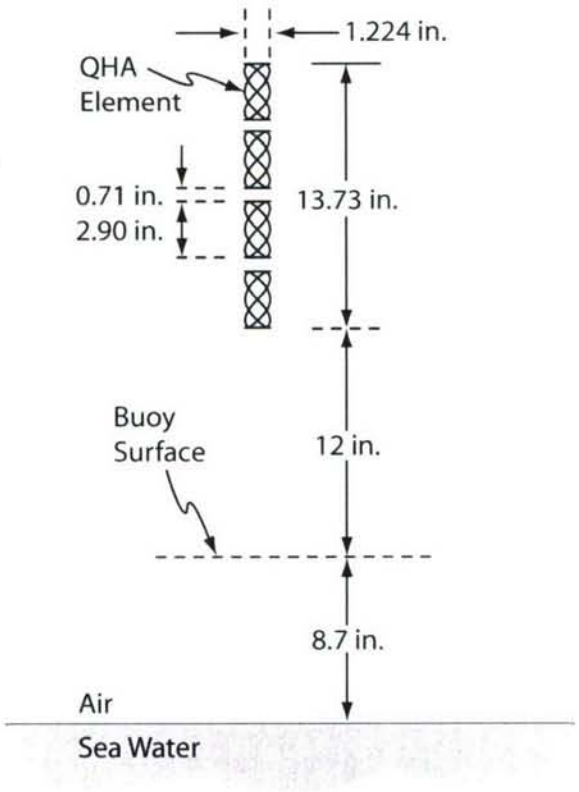

Figure 4-1. Four-Element Linear Array of QHA Elements Describing (a) Installation on a Buoy and (b) Array Geometry with Dimensions of Array Elements and Their Locations Relative to Buoy Surface and Air-Sea Water Interface

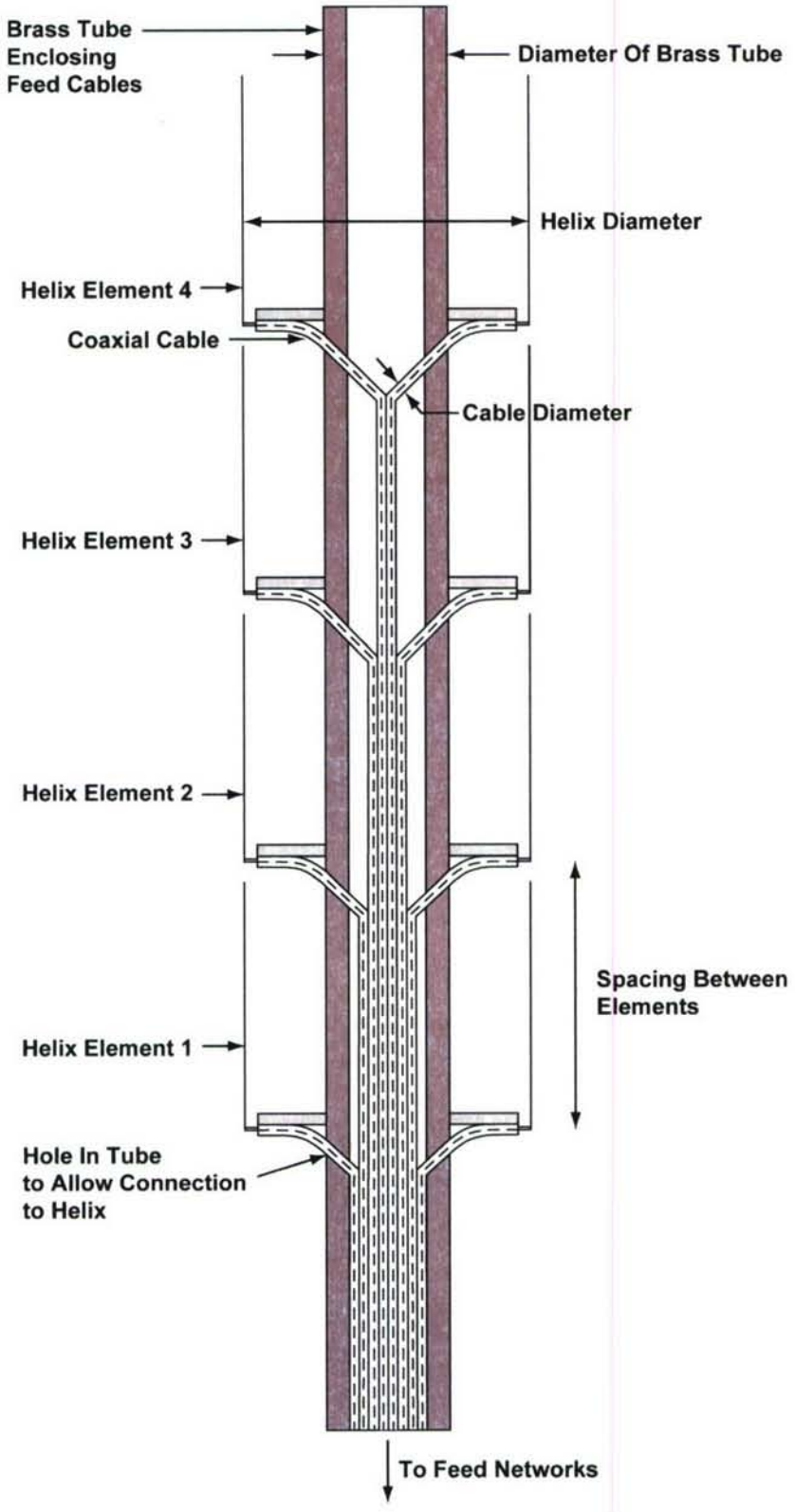

Figure 4-2. Vertical-Plane View of Feed-Cable Network for the QHA Array

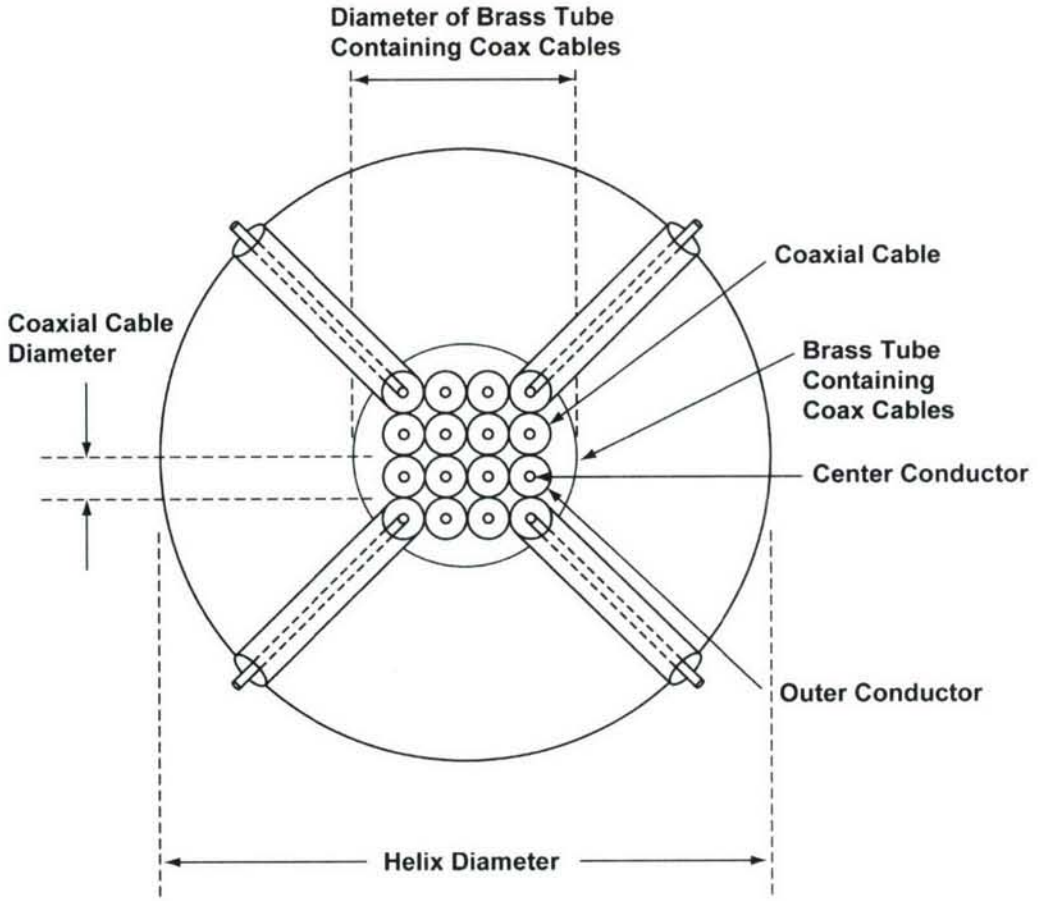

Figure 4-3. End View of Bottom Element of the QHA Array Showing Feed Cables

In the original design of the array, the brass tube and QHA array were to be constructed as a continuous piece. However, this design was determined to be difficult to assemble, especially in the attempt to pull the feed cables through the tube and slide the array of QHAs over the protruding center conductors of the feed cables. Consequently, the array was split into four separate pieces that could be assembled together.

Figure 4-4 shows a vertical-plane view of the entire array assembly, which includes the antenna elements bonded to a Mylar tube, feed cables, six sections of brass tube, and plastic spacers. Because the array elements and their associated brass-tube sections are identical, only the dimensions associated with the bottom antenna element are shown. The colors in figure 4-4 correspond to the different materials from which the array assembly is constructed. The feed tube is constructed of brass instead of copper because of its lower thermal conductivity, which allows localized heating associated with soldering. Each section of tube is stepped at an end that connects to an adjacent section of tube to provide continuity. Adjacent sections of brass tube are

attached via four set screws. There are four radial and circumferentially symmetric-spaced holes placed about the tube to allow four feed cables to connect to each QHA element. Each hole was made slightly larger than the 0.040-in. outer diameter of the feed cables to permit soldering of the cable to the hole and to avoid any possible radio frequency (RF) ground loops that may form. However, because it was determined that soldering the feed cables to the brass ring was sufficient, the cables were never soldered to the holes.

Figure 4-5 shows several QHA elements of different conductor widths that were tested to determine the strip width w that provides the proper characteristic impedance Z_0 that permits an optimum impedance match over a narrow bandwidth centered about 2.45 GHz. Each QHA in the photo was bonded to a 3-mil-thick Mylar tube. From an analysis of the measured impedances, the optimum conductor width was found to be $w = 0.24$ in., corresponding to one-half of the available space along the helical circumference. A comparison of the measured impedance data for each conductor width is given in section 5.1.

Figure 4-6 shows the section of brass tube that is associated with a given antenna element. The tube includes four symmetrically placed holes for entry of the feed cables. A brass ring, attached to the tube, is soldered to each of the four feed cables and allows each helical winding of the QHA to be fed at the helical radius. Two hard plastic spacers are glued to the brass tube with a thin spacer attached to the top surface of the brass ring and a thick spacer at the upper end of the tube. The spacers are used to hold the Mylar tube in place and to maintain a constant helical radius. Holes were drilled in the thick plastic spacer to reduce the amount of dielectric loading that it has on the antenna. Dielectric loading can produce the undesirable effect of increasing the amount of radiation in the backside direction. In the original design, the top spacer was made thick to support the ends of two adjacent Mylar tubes. However, in the current design, because the thick spacer only supports the top of one Mylar tube (corresponding to one QHA), the thickness of this spacer may be reduced.

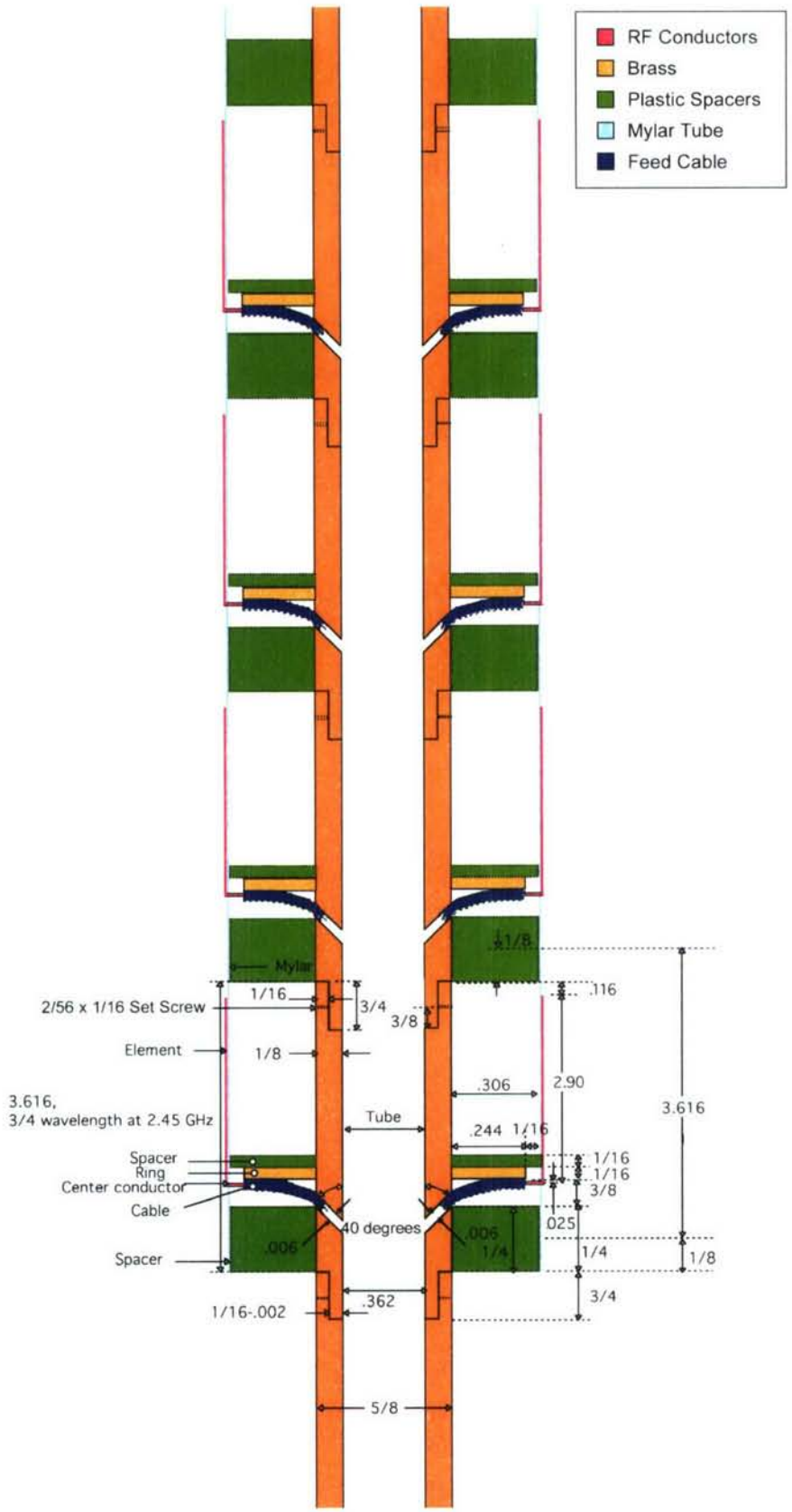

Figure 4-4. Four-Element QHA Array Assembly

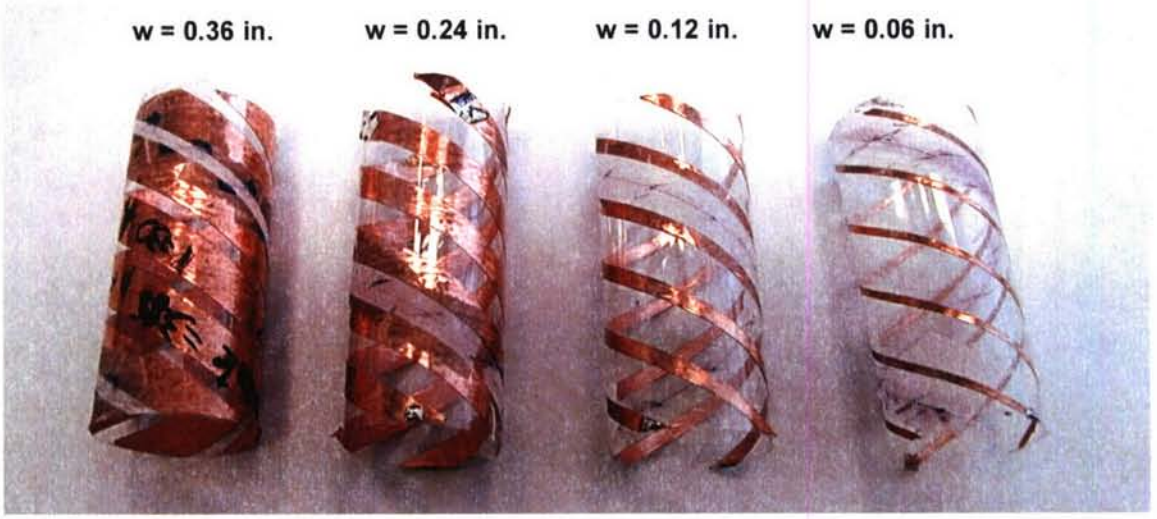

Figure 4-5. QHAs of Different Conductor Widths

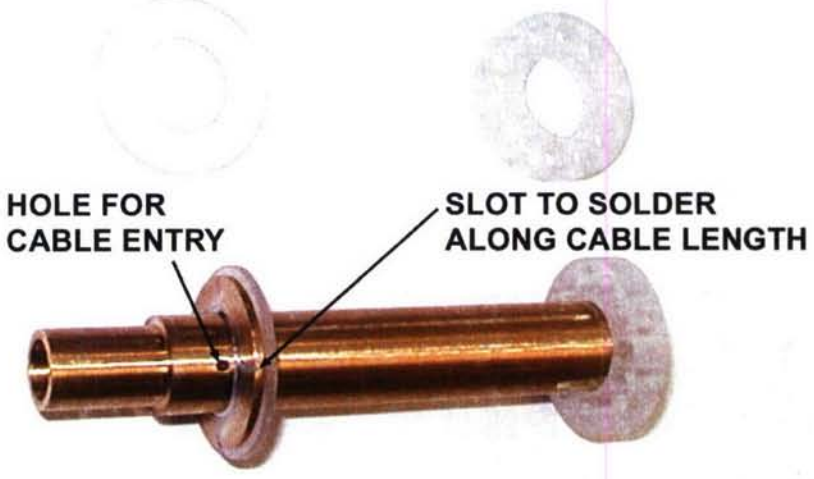

Figure 4-6. Section of Brass Tube Assembly and Plastic Spacers Associated with a QHA Element

Figure 4-7 is a photo of a QHA element and its associated feed network of power splitters. The feed network consists of an input 90° power splitter with its output ports connected to two 180° power splitters. The four output ports of the pair of 180° power splitters provide a quadrature feed for the antenna. Note that this feed network is identical to the one used for the

preliminary constructed QHA shown in figure 3-6b. The measured circuit and radiation characteristics of this QHA element in free space are presented in section 5.2.

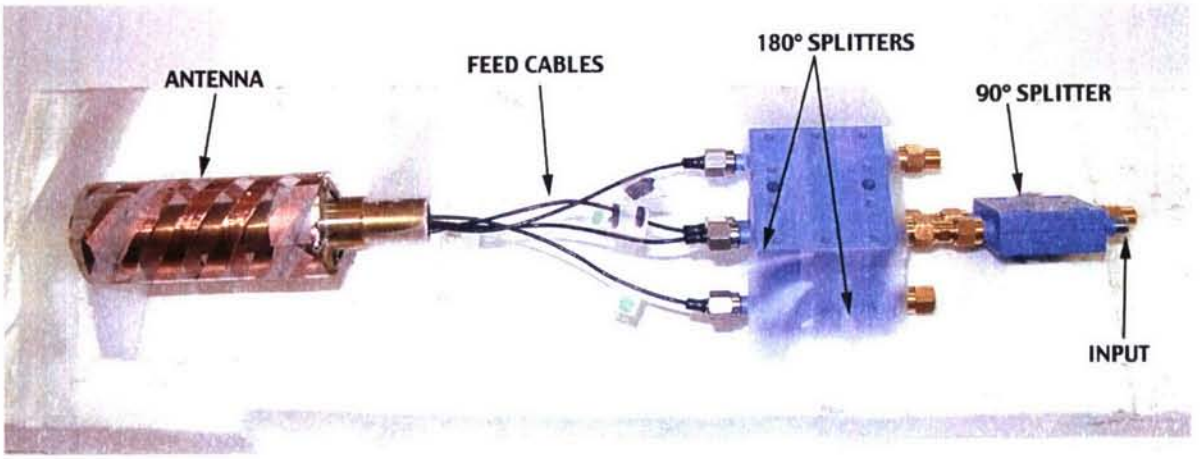

Figure 4-7. QHA with Quadrature Feed Network of Power Splitters

Figure 4-8 gives a closeup view of the feed region of one helical winding of a QHA. The photo shows that the outer jacket of the feed cable is removed to solder the outer conductor of the cable to the brass ring. The soldering of the cable outer conductor to the ring helps to establish the outer edge of the ring as the location of one end of the feed point. The other end of the feed point is the connection of the cable center conductor to the helical element. This procedure helps to prevent any RF ground loops that may be produced that could induce undesirable currents along the brass tube. Figure 4-9 is a closeup view of an interior QHA element in the array.

Figure 4-10 is a photo of the entire QHA array assembly, which includes the four antenna elements and 16 feed cables and the four element support structures, one bottom tube extension, and one top tube extension. The dimensions and construction of this array are consistent with the drawing in figure 4-4. The array elements are numbered sequentially from 1 to 4, where elements 1 and 4 denote the bottom and top elements, respectively. The 16 RF feed cables of the array are of identical length in order that the losses associated with each element are the same and that the impedance measurements for each element are referenced to the same point on a Smith chart.

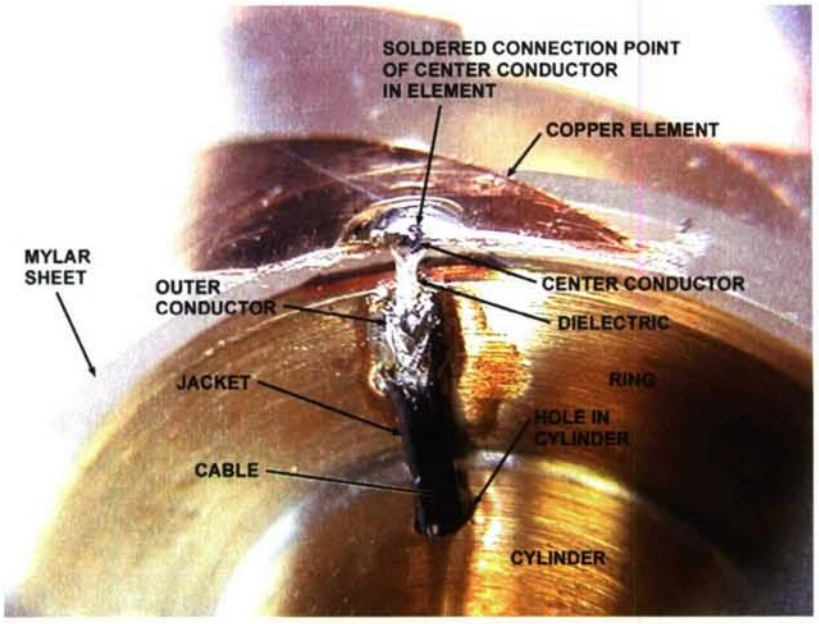

Figure 4-8. Closeup View of Element Feed Region

Figure 4-9. Closeup View of QHA Element Showing Feeds and Spacers

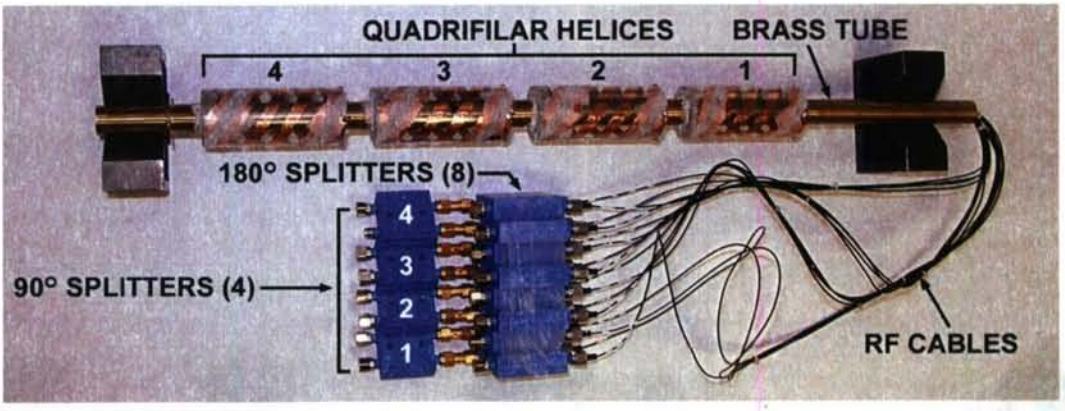

Figure 4-10. QHA Array with Feed Assembly

Figure 4-11a is a photo of the QHA array mounted to the buoy plate. A Styrofoam ring spacer is attached to the top section of the brass conduit to allow for installation of the radome (over the array) without causing damage to the helices. A 10-in. long Teflon tube, attached at the top to the lower section of the brass conduit, is designed to fit within an aluminum sleeve at the bottom to permit adjustment of the height of the array above the buoy. The aluminum sleeve is fitted with a flange to bolt the array assembly to the buoy plate. A rack is attached to the bottom of the buoy plate to mount the electronics package required for the at-sea demonstration. Figure 4-11b is a photo of the array with the radome attached. The radome consists of a thin (1/16-in. thick) tube of G-10 fiberglass with an outer diameter of 1.75 in. and a circular cap attached at the top to protect the array from exposure to the harsh sea water environment. The measured results presented in section 5.4 show that the radome has only a minor effect on the circuit and radiation characteristics of each QHA element.

Figure 4-11c shows the RF electronics associated with the QHA array that is mounted to the lower surface of the buoy plate. To collect the data necessary to provide a first-order estimate of performance that could be expected from the array and receive beamformer, the received signal envelope from each of the elements was measured as a function of time. The magnitude of the envelope is expected to vary with the presence of multipath signals. It is critical that the only contributions to the recorded signal are due to the signals of interest, namely those associated with the direct and reflected paths. Because the bandwidth of the antennas is relatively wide, the output of each antenna was fed into a bandpass filter centered at 2.452 GHz with a bandwidth of 22 MHz. The signal was then amplified to bring it into the range of the envelope detector. A low-pass filter (LPF) with cutoff frequency of 100 Hz was mounted at the bottom of the assembly for possible use in the signal detection. A comparison of the measured output of the detector with the same signal after going through the LPF indicated no appreciable difference in the output. Consequently, the LPFs were not utilized during testing of the array. The signals were digitized and recorded on a laptop computer for later analysis. Figure 4-11d is a photo of the QHA array sitting above the buoy prior to a sea test of the array in Narragansett Bay. Once the batteries and laptop computer were installed inside the buoy, the array was then bolted to the buoy. The results of the sea test are presented in another report by the authors (reference 1).

(a)

(b)

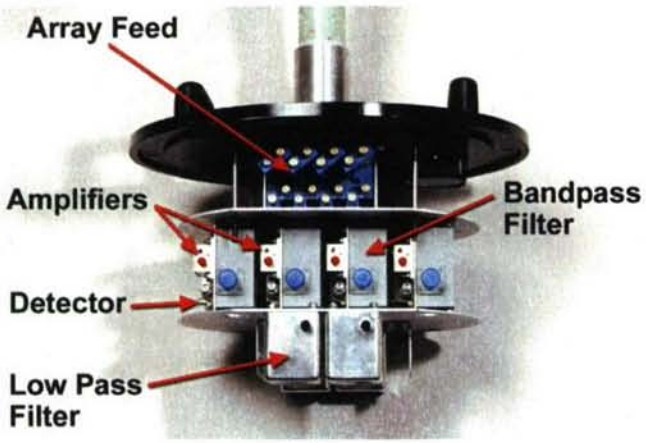

(c)

(d)

Figure 4-11. (a) QHA Array Mounted to Buoy Plate Without Radome, (b) QHA Array Mounted to Buoy Plate with Radome, (c) RF Electronics Mounted Below Buoy Plate, and (d) QHA Array and Buoy

5. MEASURED CIRCUIT AND RADIATION CHARACTERISTICS OF THE QHA ARRAY IN FREE SPACE

The previous section provided a detailed description of the design of the four-element linear array of QHAs to be used for LOS communications above the ocean surface. This design was the result of an extensive analytical and experimental effort. In this section, some experimental results are presented to provide some justification for both the element and array design parameters that were chosen. In particular, the effects of the conductor width and brass tube on the input impedance and radiation characteristics of a QHA element are presented. In addition, the effects of interelement mutual coupling, radome diameter, and buoy plate on the circuit and radiation characteristics of each array element are presented. The circuit and radiation characteristics presented in this section were measured in a free-space environment and taken at both the NUWC Division Newport Compact Range and Anechoic Chamber measurement facilities. Measurements of the QHA array when placed in a buoy above sea water are presented in another report written by the authors (reference 1).

5.1 EFFECT OF CONDUCTOR WIDTH ON THE INPUT IMPEDANCE OF A QHA ELEMENT

Figure 4-5 is a photo of four QHAs of different conductor widths (without feed assembly) that were measured to determine the conductor size that provided the best impedance match over a narrow bandwidth about the center frequency of 2.45 GHz. Each of the QHAs in figure 4-5 are open-circuited at the end (opposite the feed) with a helical diameter of 1.224 in., a 30° pitch angle, an axial length of 2.71 in., and a helical conductor length of approximately 1.25 λ at the center frequency of 2.45 GHz. Note that these dimensions are consistent with the optimum parameters chosen at the conclusion of the analysis in section 3. The labels above each QHA in figure 4-5 denote the conductor widths in inches. Note that for the QHA with the narrowest conductor width (w = 0.06 in.), the helical elements occupy approximately one-eighth of the available space along the helical circumference. In comparison, for the QHA with the widest conductor width (w = 0.36 in.), the helical elements occupy three-quarters of the available surface area.

Figure 5-1 illustrates a planar view of a helical conductor of width w that is wrapped around a circular cylinder at a pitch angle α. In figure 5-1, the parameter w_p is the conductor width projected onto the helical circumference and is related to w as follows:

$$w = w_p \sin \alpha . \tag{5-1}$$

Let D denote the helical diameter and γ be the fraction of the space along the helical circumference that is occupied by the QHA conductors. Therefore, w_p is given by

$$w_p = \frac{\gamma \pi D}{4} , 0 < \gamma < 1 . \tag{5-2}$$

The substitution of equation (5-2) into (5-1) yields

$$w = \frac{\gamma \pi D}{4} \sin \alpha , \ 0 < \gamma < 1 . \tag{5-3}$$

In figure 4-5, the helical conductor widths w = 0.06 in., 0.12 in., 0.24 in., and 0.36 in. correspond to γ = 0.125, 0.25, 0.50, and 0.75, respectively.

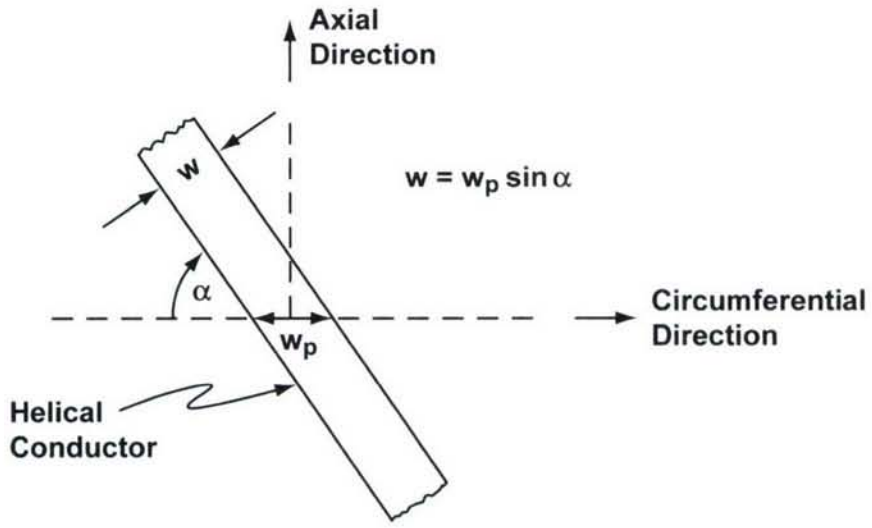

Figure 5-1. Planar View of the Geometry of a Helical Conductor of Width w Wound at a Pitch Angle α Around a Circular Cylindrical Surface

Figure 5-2 is a plot of the measured VSWR of each QHA shown in figure 4-5, each with an enclosed section of brass tube of length 4.366 in. and outer diameter of $\frac{5}{8}$ in. The brass tube used in these measurements corresponds to one interior section of the array brass tube like the one shown in figure 4-6. The VSWR was measured with a 5-in. length of coaxial cable of 0.040-in. outer diameter that was inserted between the antenna feed point and the 180° power splitters (figure 4-7). The impedance measurement point was calibrated at the 0° and 180° ports of the 180° splitters, and the reference plane for these measurements was moved to the antenna feed point. Small losses in the feed cables produce a minor decrease in the VSWR resulting in a small increase in impedance bandwidth. These losses were not accounted for in figure 5-2.

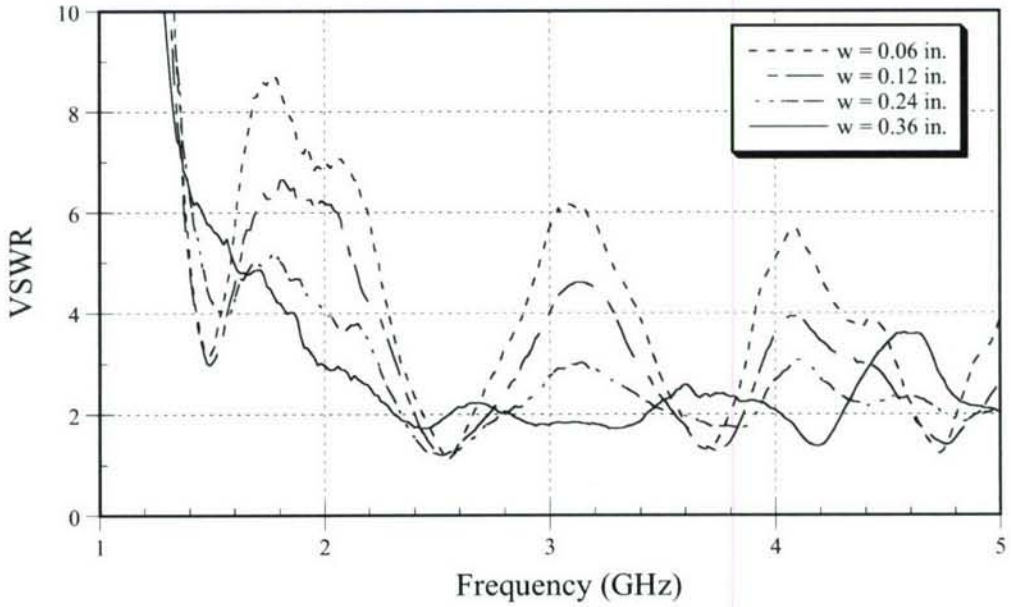

Figure 5-2. VSWR as a Function of Frequency of a QHA Element with Enclosed Brass Tube for Various Conductor Widths

The above plots show that the VSWR tends to decrease as the element width increases. This also indicates that the impedance bandwidth of the antenna increases with an increase in the conductor width. This was not observed in the computed results for a QHA that was modeled with radial feeds and, thus, without an enclosed tube, where the thin-wire helical conductors that were modeled showed a wide impedance bandwidth (or equivalently, low VSWR) above the cut-in frequency. A reduction in the conductor width increases the inductance per unit length of each helical element, which increases the characteristic impedance Z_0 of the QHA. As a result, a decrease in the conductor width causes the impedance locus (on a Smith Chart) above the cut-in

frequency to move to the right and to rotate clockwise (in the inductive direction), thereby moving the center of the locus off of the real axis. This additional inductance results in a reduction in the impedance bandwidth of the QHA. This portion of the impedance locus also spreads out somewhat with decreased element width and contributes to a decrease in bandwidth. Because wider elements occupy more space, they result in more impedance bandwidth.

The effect of the enclosed brass tube on the impedance of the QHA can be observed through a comparison of the above VSWR plots with figure 3-7b. It should be recalled that figure 3-7b was measured for a QHA of the same dimensions as the above antennas with a wide-conducting element of width $w = 0.43$ in. ($\gamma = 0.9$) without an enclosed tube. A comparison of figure 3-7b with the VSWR plot of the widest element in figure 5-2 (i.e., $w = 0.36$ in.) indicates that the introduction of the brass tube results in a noticeable reduction in impedance bandwidth. It should also be mentioned that some of this reduction in bandwidth is attributed to the narrower conductor widths that were measured in figure 5-2.

Figure 5-3 shows Smith charts of the input impedance of the quadrifilar helices described above for helical conductor widths $w = 0.24$ in. and $w = 0.36$ in. The Smith charts are for one bifilar arm and are normalized by the characteristic impedance $Z_0 = 100$ ohms. The Smith charts suggest that the optimum frequency for impedance match to Z_0 is approximately 2.50 GHz. The minimum VSWR for each of the plots in figure 5-2 also occurs at approximately 2.50 GHz, indicative of an optimum impedance match. The Smith charts in figure 5-3 show that the narrower conductor provides a better impedance match (i.e., closer to Z_0) at 2.50 GHz than the wider conductor, but unfortunately results in less bandwidth. A decrease in the conductor width causes the impedance locus in the Smith Chart to move to the right, rotate slightly clockwise in the inductive direction, and spread further apart. The impedance measurements for the four conductor widths suggest that the optimum conductor width is between $w = 0.12$ in. and $w = 0.24$ in., or approximately $w = 0.18$ in., equivalent to $\gamma = 0.375$. However, because a wider conductor results in greater bandwidth and because it is desirable to have sufficient bandwidth to allow for the possibility of small impedance changes from construction variability and radome loading, in addition to mutual-coupling effects when the antenna element is placed in the array, the conductor width selected for the current design, $w = 0.24$ in., is a little wider than the optimally matched case.

(a)

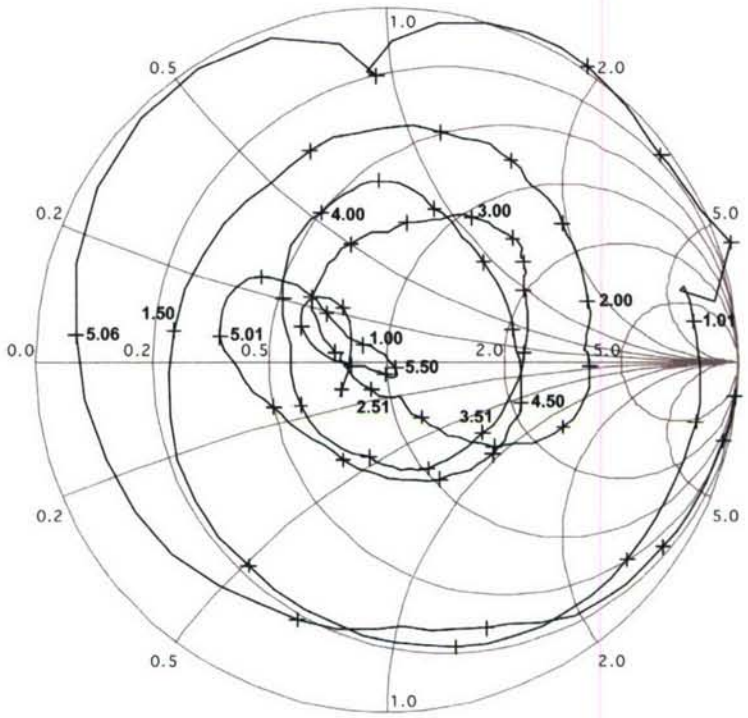

(b)

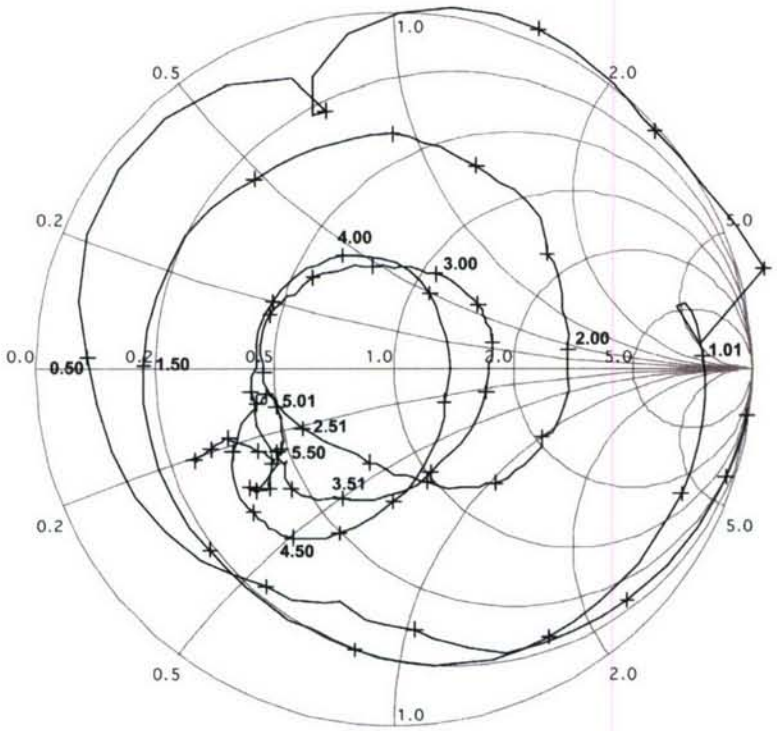

Figure 5-3. Smith Chart of the Measured Input Impedance of One Bifilar Pair of a QHA Element (Pitch Angle = 30°, Diameter = 1.224 in., Axial Length = 2.71 in.) with an Enclosed Section of Brass Tube for Different Conductor Widths: (a) w = 0.24 in. and (b) w = 0.36 in.

The above results have shown that the optimum impedance match occurs at approximately 2.50 GHz, which is 50 MHz higher than the design frequency of 2.45 GHz. This slightly higher frequency is attributed to the reduction in the element length that resulted when the feed point was displaced from the helical axis out to the circumference of the antenna with the introduction of the brass radial ring. Consequently, to achieve an optimum impedance match at the design frequency of 2.45 GHz, the element length was increased by a small amount, resulting in an increase in the element axial length from 2.71 in. to 2.90 in. This increase in element length was determined via experiment. The measured results for the final element design are presented in section 5.2.

5.2 QHA ELEMENT—FINAL DESIGN

The above results described the process for determining the final design parameters for the QHA element to be used in the linear array. The final design parameters chosen are listed in table 5-1. In addition, the antenna element is fed at its circumference (figure 4-8) by four coaxial cables that emanate from an enclosed section of brass tube of ⅝-in. outer diameter as described in figure 4-4. Figure 4-7 shows a QHA with the final design parameters with its network of power splitters. The assembly shown in figure 4-7 was the one used to obtain the circuit and radiation characteristics of the final QHA element design in free space that is described below. Figure 4-9 provides a closeup view of the final element design.

Table 5-1. Design Parameters of QHA Element

Pitch Angle	Helical Diameter	Axial Length	Conductor Width
30°	1.224 in.	2.90 in.	0.24 in.

Figure 5-4a shows the measured free-space radiation patterns in the vertical plane of a QHA element with an enclosed brass feed tube. The patterns show that the antenna produces a pattern with a wide beamwidth and maximum radiation overhead ($\theta = 0°$) that is predominantly right-hand circularly polarized (RHCP) in the upper half-space and left-hand circularly polarized (LHCP) over most of the lower half-space. Although the radiation in the lower half-space is primarily LHCP, the gain in this region is significantly lower than the RHCP gain produced in the

upper half-space. It should be noted that when this antenna is located above sea water, the LHCP wave that is incident onto the air-sea water interface will be reflected as an RHCP wave into the upper half-space and combine with the RHCP direct wave to produce multipath interference. The large ratio of RHCP gain at a given incident polar angle θ in the upper half-space to the LHCP gain at the corresponding incident angle in the lower half-space (i.e., $180° - \theta$) indicates that the QHA element is fairly immune to multipath interference when placed above sea water. Because the radiation pattern is nearly axisymmetric, the pattern is plotted in only one vertical plane.

Figure 5-4b shows plots of the measured VSWR at the feed points of both bifilar elements of a QHA with an enclosed brass feed tube. The plots indicate that the antenna has a good impedance match at 2.45 GHz with a VSWR = 1.3. It should be noted that a VSWR of 3 results in an impedance mismatch loss of approximately 1.25 dB and the VSWR = 1.3 at 2.45 GHz produces an impedance mismatch loss of about 0.75 dB. Figure 5-5 is a Smith chart of the impedance loci of the two bifilar arms of the QHA element. Figures 5-4b and 5-5 show that the two bifilar arms have nearly equal input impedance and VSWR over most frequencies plotted.

Impedance and radiation pattern measurements were also made of a QHA element with an additional section of brass tube attached above it. These measurements were performed to determine if a longer length of tube would have any effect on the circuit and radiation characteristics of the QHA. The measurements showed that the added section of brass tube produced only a slight change in the measured impedance of the antenna and had no noticeable effect on the element radiation pattern. Therefore, when each QHA element is placed in the linear array configuration in figure 4-4, the added length of brass tube is not expected to have any major effect on the impedance and radiation pattern of each element.

(a)

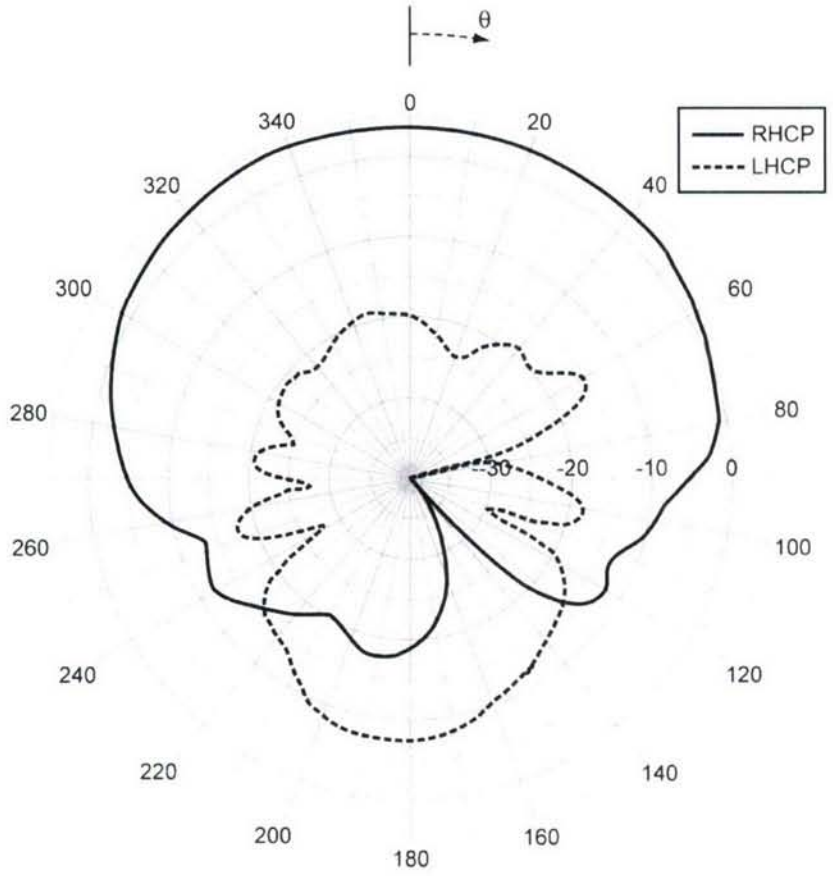

(b)

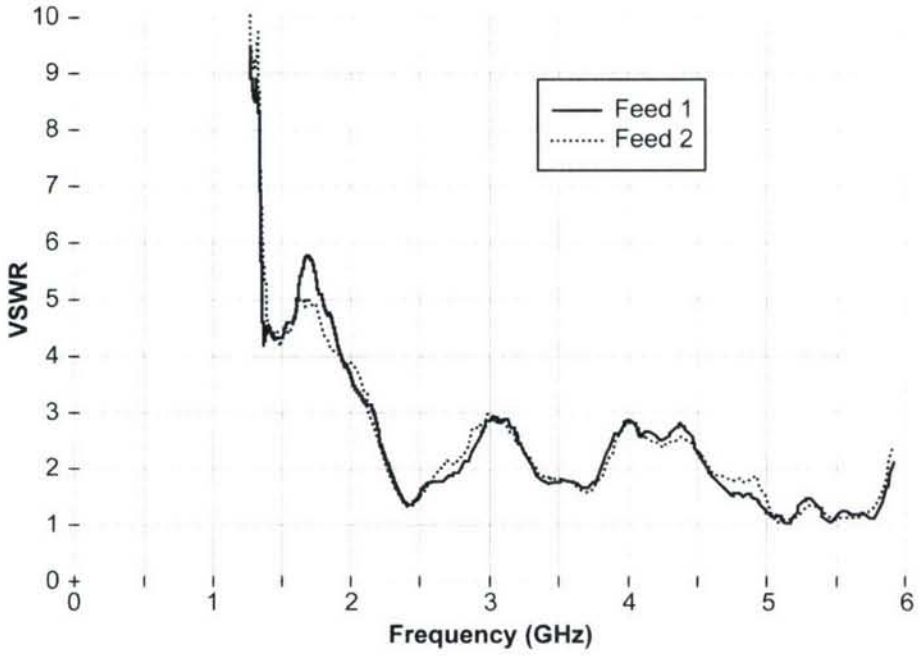

Figure 5-4. QHA Element Measured with Brass Tube: (a) Gain Patterns in dB and (b) VSWR of Both Bifilar Feed Arms

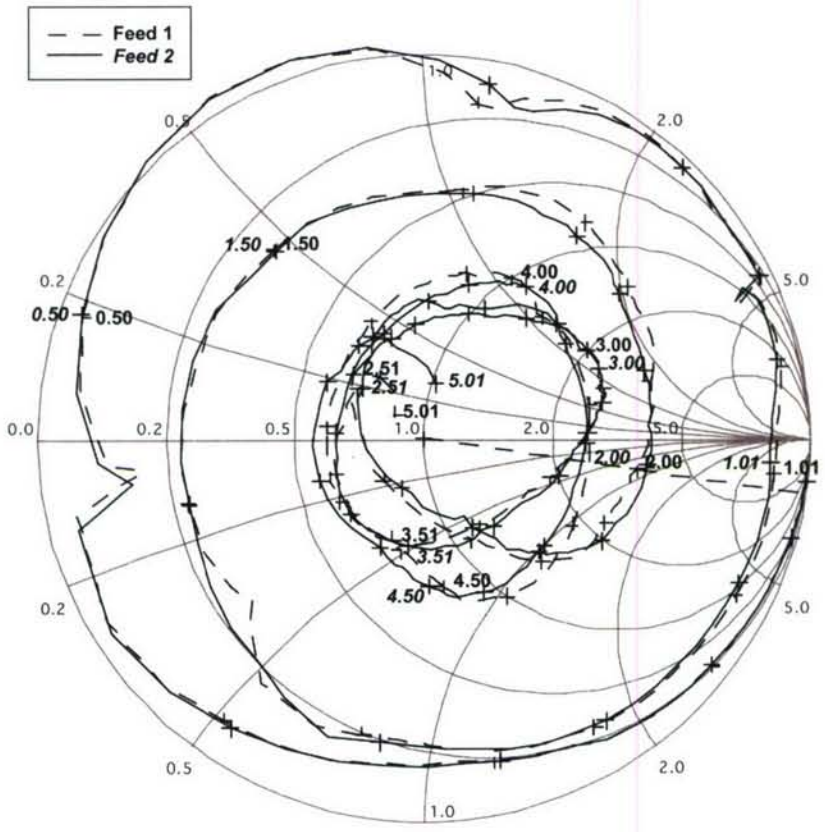

Figure 5-5. Smith Chart of the Measured Input Impedance of Both Bifilar Feeds of the Final QHA Element Design (Pitch Angle = 30°, Diameter = 1.224 in., Axial Length = 2.90 in. with an Enclosed Section of Brass Tube

5.3 MEASUREMENT OF QHA ELEMENTS IN THE ARRAY CONFIGURATION

The graphs in the previous section indicate that the QHA element has an input impedance that is properly matched at the 2.45-GHz design frequency and produces a radiation pattern that indicates good immunity with respect to multipath. Following the measurement of a QHA element in free space, measurements were made of the free-space circuit and radiation characteristics of each of the four QHA elements when placed in the array configuration. Figure 4-10 is a photo of the array with feed assembly that was measured in NUWC Division Newport's compact range facility. In the measured data that follows, note that the array elements are numbered sequentially with elements 1 and 4 referring to the bottom and top elements, respectively, in the array.

Figure 5-6 shows the RHCP and LHCP measured element patterns of the QHA array in free space. The pattern of each element was measured separately while it was positioned within

the array configuration with the ports of the other elements terminated in matched 50-ohm loads. As a result, the measured patterns account for the effects of mutual coupling between the array elements, corresponding to the at-sea case where each array element is terminated at the input of a receiver. A comparison of these patterns with the element patterns in figure 5-4a indicates that each QHA element suffers a reduction in overhead gain when it is placed in the array. This reduction in gain is attributed to the added losses in the longer feed cables used in the array and from the mutual coupling between the elements. The overhead gain (–4.23 dB) of the lowest element (1) is reduced by the greatest amount while the overhead gain (0.44 dB) of the highest element (4) is reduced by the least from when it is isolated (3.4 dB). The larger reduction in gain for the lower elements is expected because each QHA is excited in the forward-fire mode and the larger intensity fields produced in the forward direction will couple power to any antennas that are located above, where the coupled power can be dissipated in the terminations of these antennas. The front-to-back gain ratios for elements 1, 2, 3, and 4 are 5.3 dB, 5.6 dB, 7.5 dB, and 10.7 dB, respectively. These ratios are smaller than the 11-dB value measured for an isolated QHA element and indicate that the bottom array elements are more susceptible to multipath interference than those on the top of the array.

Figure 5-7 is a plot of the measured VSWR of one bifilar element of QHA array elements 1 and 2 as a function of frequency. The VSWR plots of the other bifilar pairs of these elements show similar variation and therefore are not shown. It should be noted that these plots have more error than the VSWR plot of an isolated element in figure 5-4 because of the longer cables connected to the elements in the array configuration. Unfortunately, the reflections and losses in the cables could not be calibrated out of the measurements. Consequently, the reflections in the cables appear as ripple in the VSWR plots, and the losses in the cables result in somewhat lower VSWR than that measured for an isolated QHA element. The plots show that the VSWR is less than 2 over most of the frequency band extending from 1.8 GHz to 5 GHz. At the center frequency of 2.45 GHz, the VSWRs of elements 1 and 2 are approximately 1.7 and 1.9, respectively. In comparison, from figure 5-4, the VSWR of an isolated QHA at 2.45 GHz is approximately 1.5.

Figure 5-8 shows plots of the total antenna efficiency of each QHA element as a function of frequency over the 2.2 to 3 GHz frequency band. The antenna efficiency is defined as the ratio of the total power radiated to the total input power to the antenna (reference 9). The plots in figure 5-8 were determined through integration of the measured gain patterns associated with the

(a)

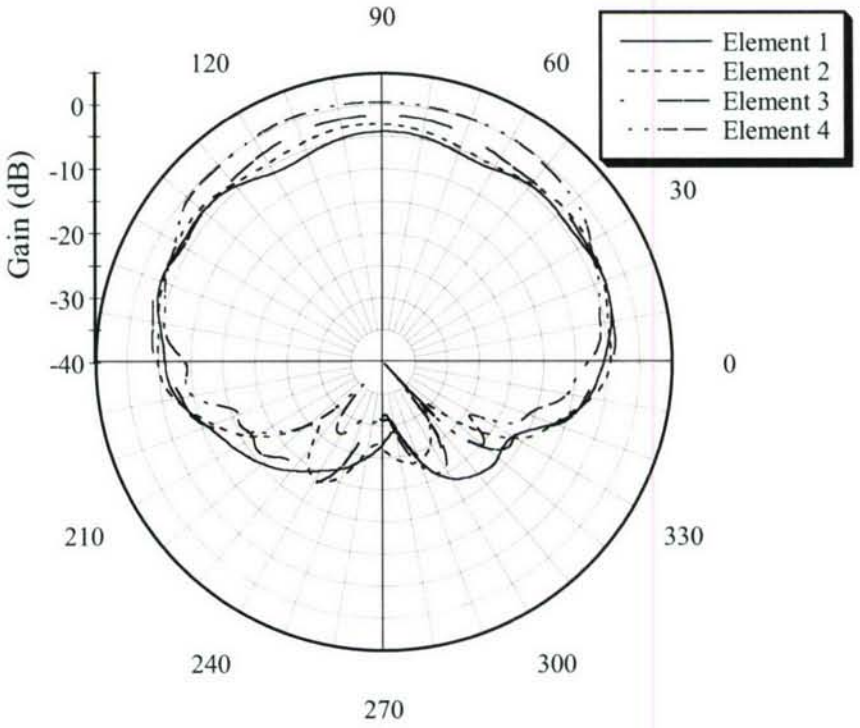

(b)

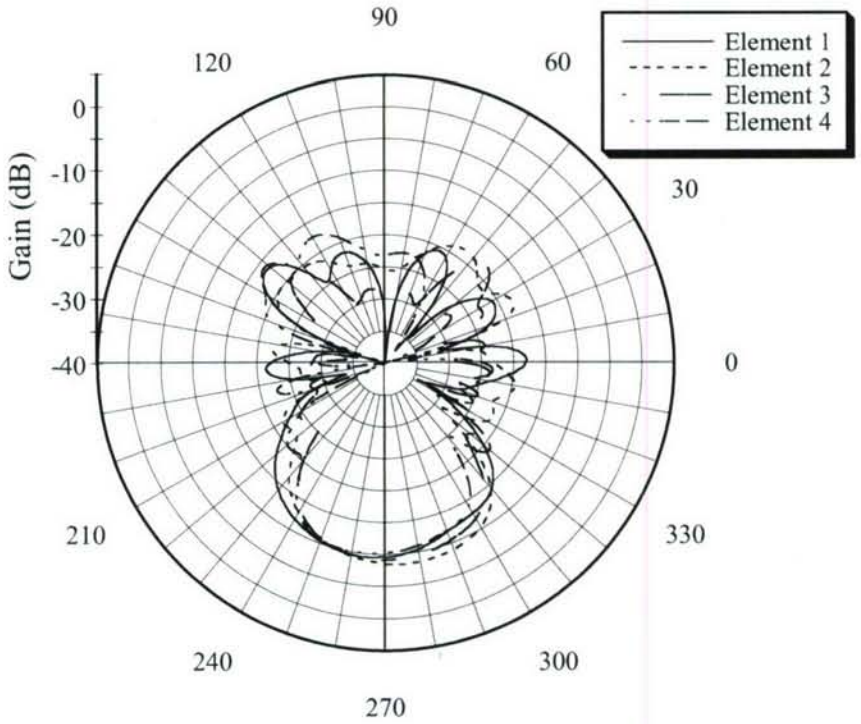

Figure 5-6. Measured Gain Patterns of QHA Array Elements in Free Space: (a) RHCP or Copolarized Component and (b) LHCP or Cross-Polarized Component

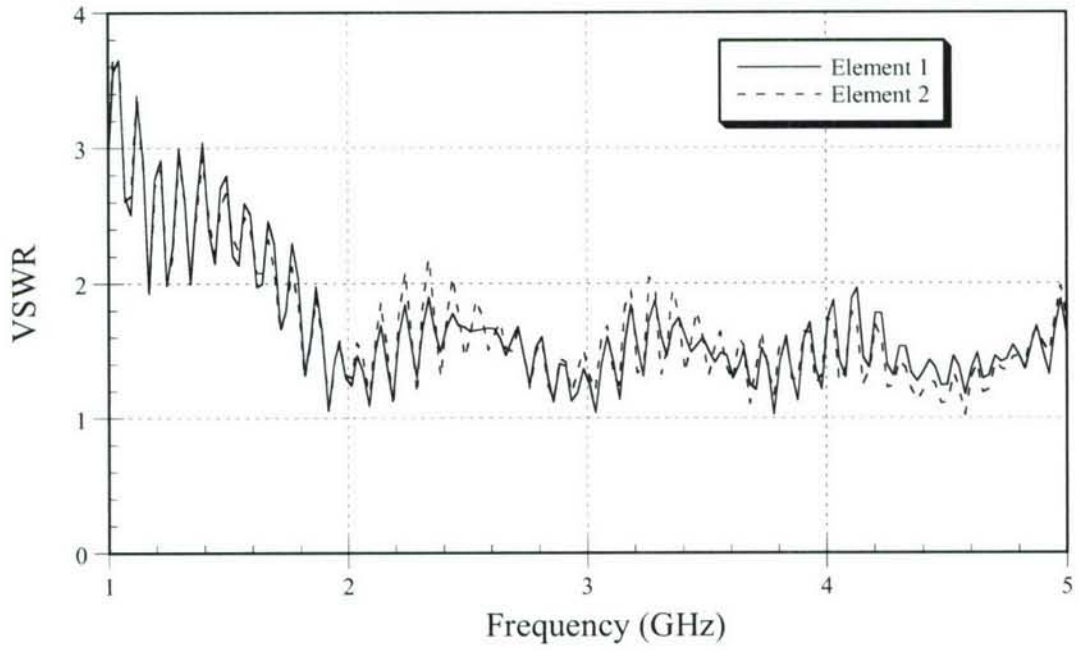

Figure 5-7. Measured VSWR as a Function of Frequency of One Bifilar Feed of the Two Bottom QHA Array Elements in Free Space

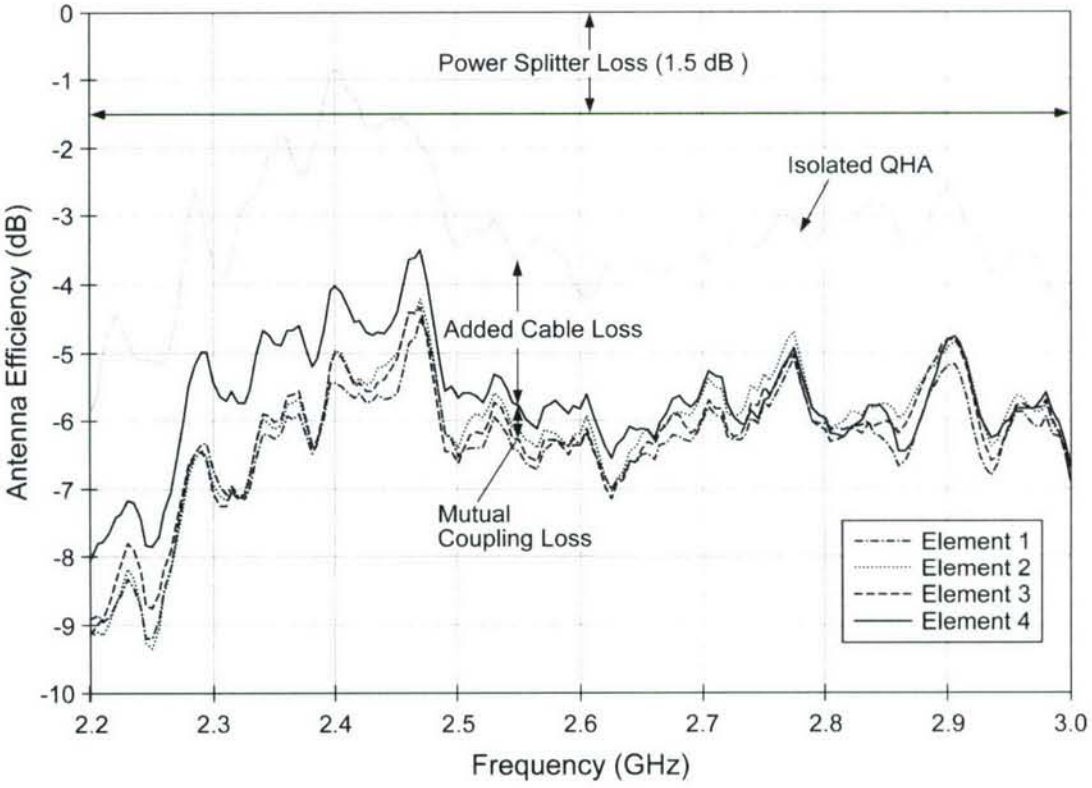

Figure 5-8. Losses Associated with Power Splitters, Impedance Mismatch, and Mutual Coupling for the QHA Array Measured in Free Space

vertical and horizontal field components produced by each element, adding the results and dividing by 4π. Therefore, the element efficiencies plotted in figure 5-8 denote the total losses that are attributed to the power splitters, impedance mismatch, feed cables, and interelement mutual coupling. Over the 2.2- to 3-GHz frequency band, the measured loss associated with the power splitters is approximately 1.5 dB. At 2.45 GHz, the loss associated with each 30-in. long feed cable in the array is 1.1 dB/ft x 2.5 ft = 2.75 dB. The difference in efficiencies between an isolated QHA and element 4 is primarily attributed to the losses from the additional length of cable used in the array. For example, at 2.45 GHz, the difference in efficiencies between an isolated QHA and element 4 is approximately 2.5 dB. The differences in efficiencies between each array element are attributed to interelement mutual coupling. Therefore, at the design frequency of 2.45 GHz, it is not surprising that the top element (4) has the highest efficiency and the bottom element (1) has the lowest efficiency.

5.4 EFFECT OF RADOME ON THE CIRCUIT AND RADIATION CHARACTERISTICS OF THE ARRAY

When the QHA array system described in figure 4-1 is deployed, the splash or spray from the sea water can cause both mechanical and RF degradation of the array. To protect the array from the sea water environment, it must be enclosed in a radome. Several 1/16-in. thick tubes of varying diameter, made of G-10 fiberglass, were considered for application as radomes. In particular, the circuit and radiation characteristics of the array were measured with fiberglass tubes of outer diameters 1.5, 1.75, 2.0, and 2.25 in. The length of each tube was 4 feet and was more than sufficient to completely cover the array.

Figure 5-9 is a plot of the measured VSWR in free space of one bifilar pair of an isolated QHA element that is centered within each fiberglass radome of varying outer diameter. The plots show that over the 2- to 3-GHz frequency band the radome has only a minor effect on the measured VSWR. In the vicinity of the center frequency of 2.45 GHz, the radome causes the minimum VSWR to shift slightly toward a lower frequency and is attributed to the dielectric loading presented by the fiberglass. This shift in frequency increases with a decrease in the tube diameter. In figure 5-9, the 1.5-in. diameter tube has the most noticeable effect on the element VSWR. From the plot in figure 5-9, the VSWR at 2.45 GHz of the antenna without the radome is approximately 1.11 as compared with 1.40, 1.12, and 1.04 when the antenna is enclosed in a

radome of outer diameter 1.5 in., 1.75 in., and 2.25 in., respectively. Consequently, a fiberglass tubular radome of outer diameter 1.75 in. or greater does not have much effect on the input impedance of a QHA element.

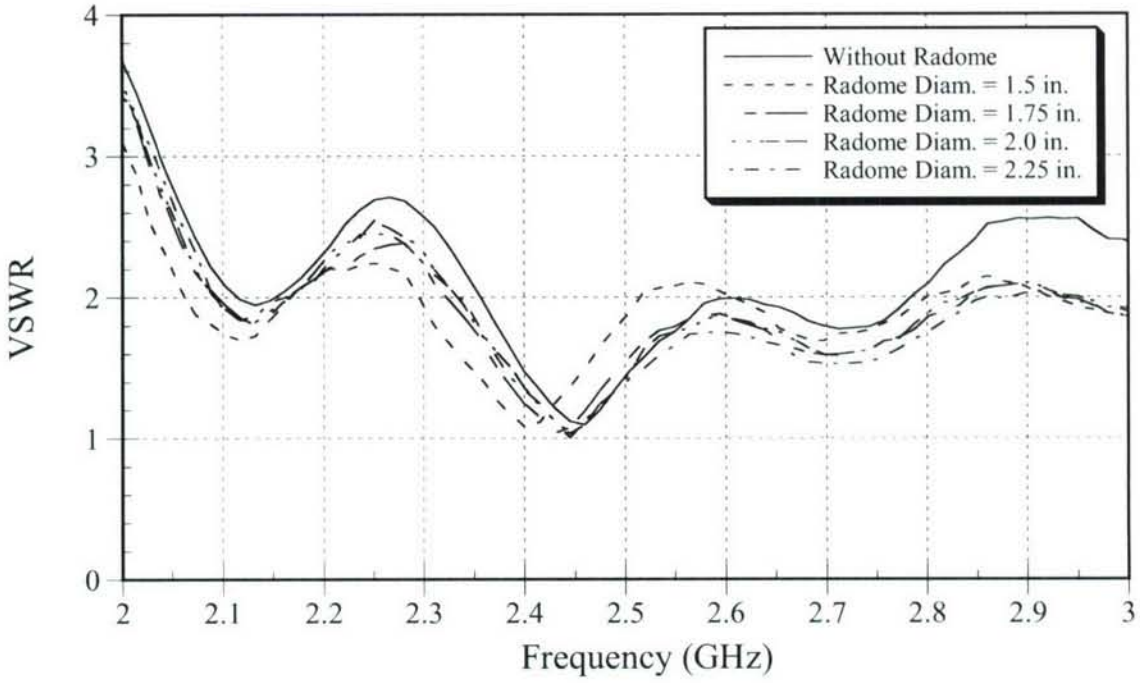

Figure 5-9. Measured VSWR as a Function of Frequency for One Bifilar Pair of an Isolated QHA Enclosed Within G-10 Fiberglass Tubes of Various Outer Diameters

Figures 5-10 and 5-11 show plots of the RHCP gain patterns of the QHA array elements enclosed in radomes of varying diameter and measured in free space. These plots show that, for each QHA element, the radome causes a small increase in the gain in the overhead direction and a small decrease in gain at lower elevation angles. The plots also show that the radome produces more ripples in the radiation pattern. These effects increase with larger radome diameter because of the additional phase differences in reflections between the antenna and radome. In conclusion, a smaller diameter radome has the least effect on the array element radiation characteristics.

(a)

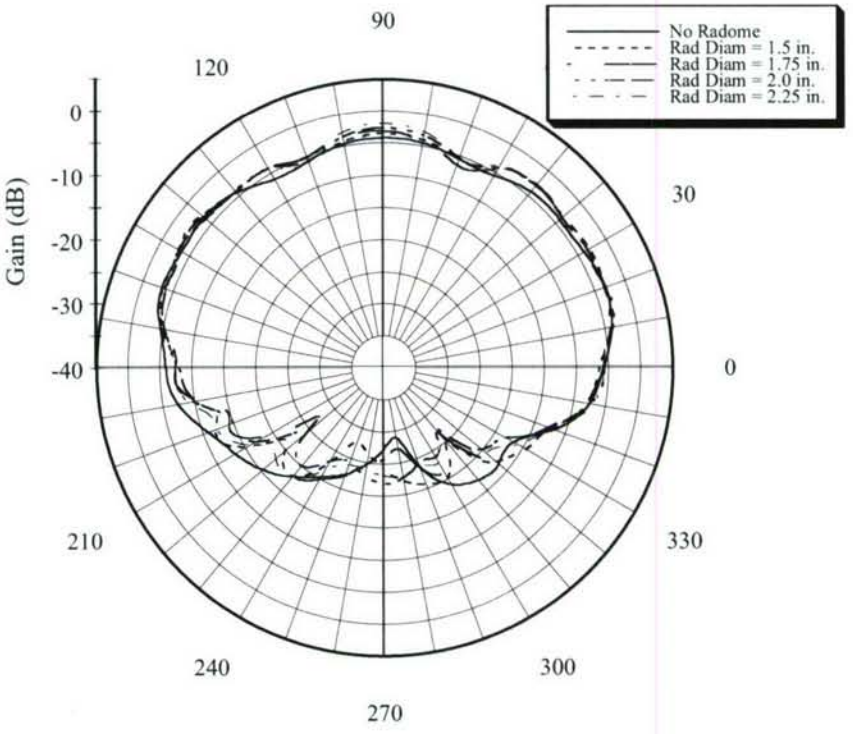

(b)

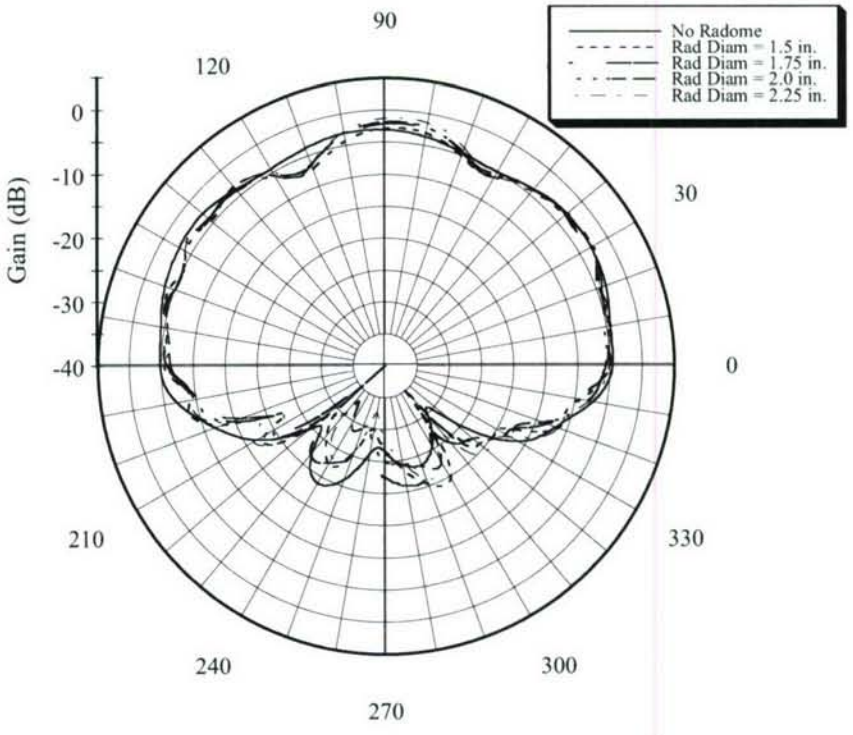

Figure 5-10. Effect of G-10 Fiberglass Radomes of Various Diameters on the Measured RHCP Gain Patterns vs Elevation Angle in Free Space of the QHA Array Elements: (a) Element 1 and (b) Element 2

(a)

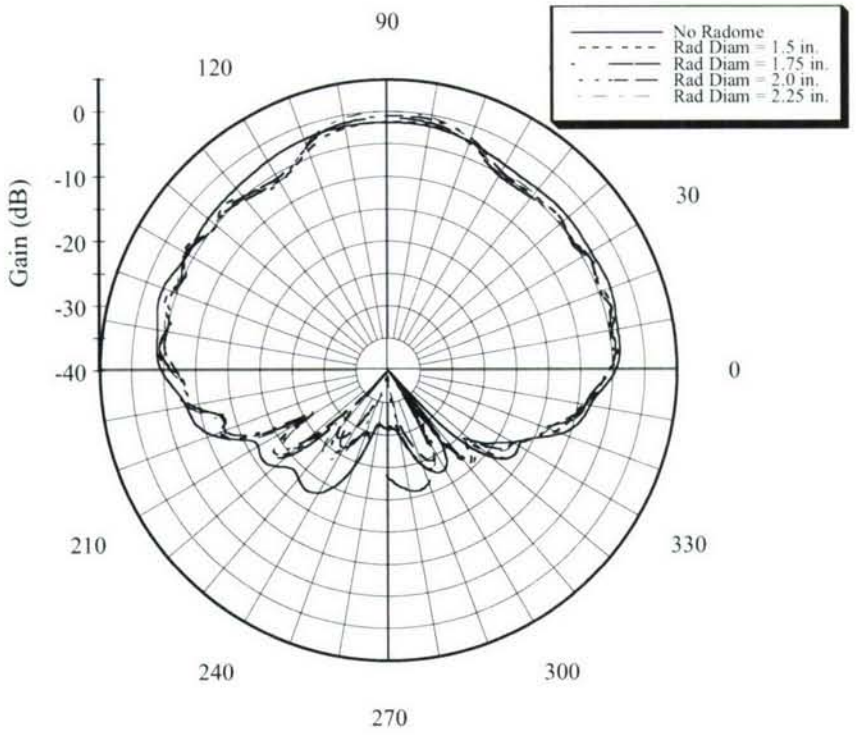

(b)

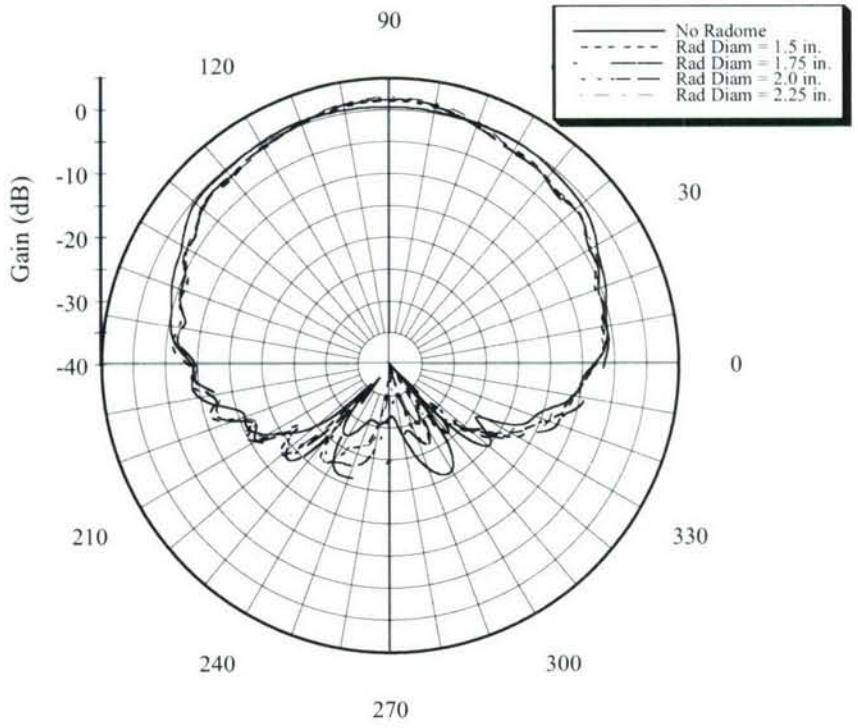

Figure 5-11. Effect of G-10 Fiberglass Radomes of Various Diameters on the Measured RHCP Gain Patterns vs Elevation Angle in Free Space of the QHA Array Elements: (a) Element 3 and (b) Element 4

The above results have shown that the smallest diameter radome has the greatest effect on the QHA input impedance, and the largest diameter radome has the most noticeable effect on the element radiation patterns. However, because of the losses in the fiberglass, a smaller diameter radome, being more coupled to the antenna, can add more loss to the antenna and reduce its efficiency. The measured results also show that the dominant effect that the radome diameter has on the antenna is on its radiation pattern. Therefore, a smaller diameter tube is preferable. In conclusion, a 1.75-in. diameter tube was chosen as the radome for the QHA array.

Figure 5-12 shows the measured RHCP and LHCP gain patterns of the QHA elements enclosed in a 1.75-in. diameter radome in free space. The pattern front-to-back ratios of elements 1, 2, 3, and 4 are approximately 8 dB, 6.5 dB, 7 dB, and 11 dB, respectively. As compared with the element patterns without the radome, these values are somewhat greater for elements 1 and 2 and are about the same for elements 3 and 4. A comparison of figures 5-6a and 5-12a, shows that the radome causes more ripples in the RHCP pattern and slightly reduced gain for elements 3 and 4 at lower elevation angles in the upper half-space.

(a)

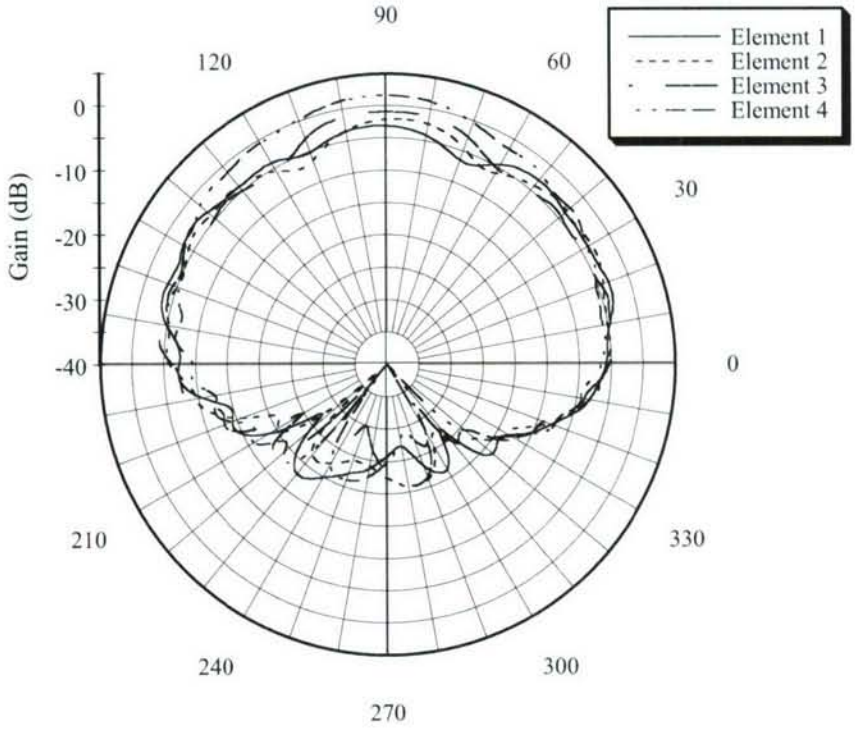

(b)

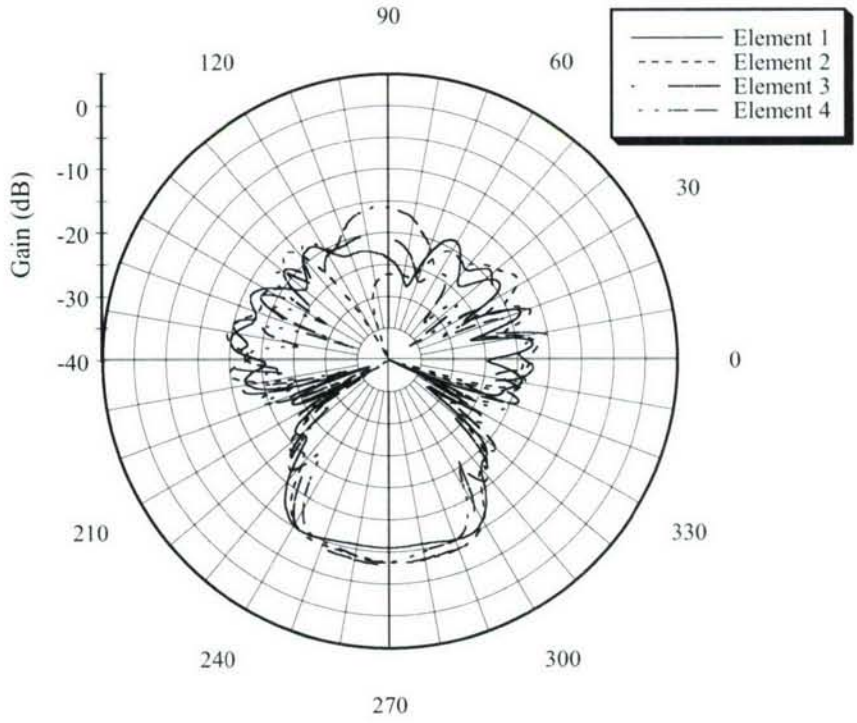

Figure 5-12. Measured Gain Patterns of the QHA Array Elements with 1.75-in. Diameter G-10 Fiberglass Radome in Free Space: (a) RHCP or Copolarized Component and (b) LHCP or Cross-Polarized Component

5.5 MEASUREMENT OF ARRAY WITH BUOY PLATE AND RF ELECTRONICS PACKAGE

Figure 4-11b is a photo of the QHA array enclosed in a 1/16-in. thick fiberglass radome with an outer diameter of 1.75 in. and mounted to the buoy plate. The radome was reduced in length to 31.75 in. and its lower end was inserted inside of a 4.25-in. long aluminum sleeve that was bolted to the top of the buoy plate. A circular cap made of G-10 fiberglass was attached to the upper end of the radome to seal it and further protect the array from the sea water environment.

Figure 5-13 shows the measured RHCP and LHCP gain patterns as functions of elevation angle in free space of each QHA element in the array with the radome and buoy plate as shown in figure 4-11b. A comparison of the element RHCP patterns in figures 5-12a and 5-13a indicates that the additional ripples in the patterns in the overhead region (in the vicinity of elevation angle = 90°) in figure 5-13a are attributed to reflections from the buoy plate. In figure 5-13a, the overhead RHCP gains of elements 1, 2, 3, and 4 are 1.33 dB, –6.76 dB, 3.29 dB, and 0.36 dB, respectively. A comparison of figures 5-12a and 5-13a suggests that the presence of the buoy plate results in an increase in the overhead gains of elements 1 and 3 and a reduction in the overhead gains of elements 2 and 4. Note that element 2 has a noticeably smaller overhead gain than the other elements. From the patterns in figure 5-13, the pattern front-to-back ratios of elements 1, 2, 3, and 4 are approximately 31.7 dB, 22.7 dB, 33.6 dB, and 29.7 dB, respectively. These ratios are much greater than for the patterns in figures 5-12 because of the significant reduction in LHCP gain in the backside direction (elevation angle = –90° or 270° in figure 5-13), which is attributed to the shielding of the array by the buoy plate.

The radiation patterns in figure 5-13 indicate that the buoy plate produces some degradation in the QHA element radiation patterns in the upper half-space because of the interference produced by reflections from the buoy plate. These undesirable reflections may be reduced by applying an RF absorbing material to the top surface of the buoy plate.

(a)

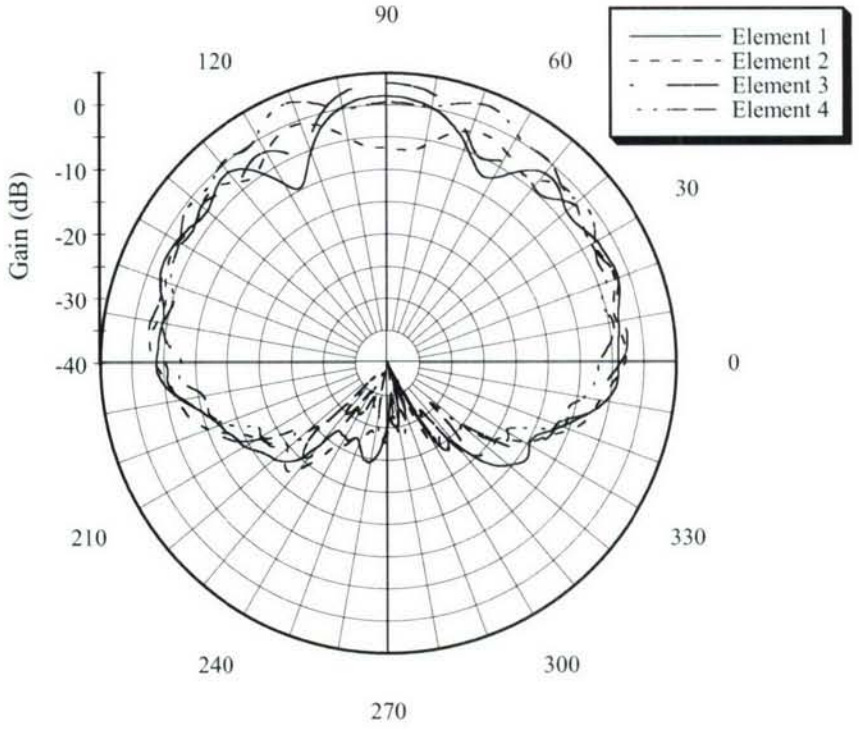

(b)

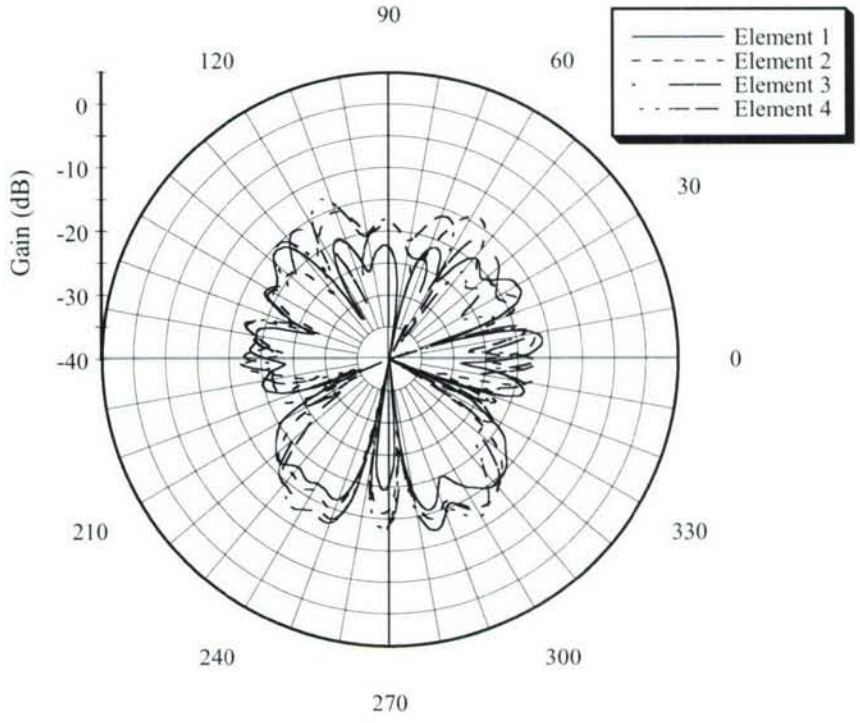

Figure 5-13. Gain Patterns vs Elevation Angle in Free Space of the QHA Array Elements Measured with Radome and Mounted to Buoy Plate as Shown in Figure 4-11b: (a) RHCP or Copolarized Component and (b) LHCP or Cross-Polarized Component

6. PREDICTED RADIATION CHARACTERISTICS OF THE QHA ARRAY ELEMENTS ABOVE SEA WATER

The measured gain patterns in free space of each QHA element in the array with the radome and buoy plate plotted in figure 5-13 were used to compute the directive gain of each element at its appropriate height above sea water. A flat sea surface was assumed in these calculations because it provides a worst-case scenario for multipath interference. From the array geometry shown in figure 4-1b, the heights of the geometrical centers of the QHA elements above the sea surface (located at $z = 0$) are given (in inches) as

$$z_n = 22.15 + (n - 1)\, 3.61,\ n = 1, 2, 3, 4\ , \tag{6-1}$$

where the index n denotes the element number. In the gain calculations, it is assumed that the element phase centers are coincident with their geometrical centers. The directive gain referenced to the RHCP field component E_R above sea water is given by

$$g_d(\theta,\varphi) = \frac{4\pi\,|\,E_R(\theta,\varphi)\,|^2}{\displaystyle\int_0^{2\pi}\int_0^{\pi/2} |\,\boldsymbol{E}(\theta,\varphi)\,|^2 \sin\theta\, d\theta\, d\varphi}\ , \tag{6-2}$$

where (θ,φ) denote the polar and azimuth angles in the spherical coordinate system described in figure 6-1, and $|\boldsymbol{E}(\theta,\varphi)|$ is the magnitude of the radiated field above sea water. An explanation of these calculations is given in reference 1.

As previously mentioned, because the radiation patterns of the QHA elements are nearly axisymmetric, the free-space patterns were measured in only one vertical plane. Consequently, the directive gain formula (6-2) reduces to

$$g_d(\theta,\varphi) = \frac{4\,|\,E_R(\theta,\varphi)\,|^2}{\displaystyle\int_0^{\pi/2} \left[\,|\,\boldsymbol{E}(\theta,0)\,|^2 + |\,\boldsymbol{E}(\theta,\pi)\,|^2\right] \sin\theta\, d\theta}\ , \tag{6-3}$$

where $\boldsymbol{E}(\theta,0)$ and $\boldsymbol{E}(\theta,\pi)$ are determined from the field components plotted on the right and left halves, respectively, of the polar plots in figure 5-13a.

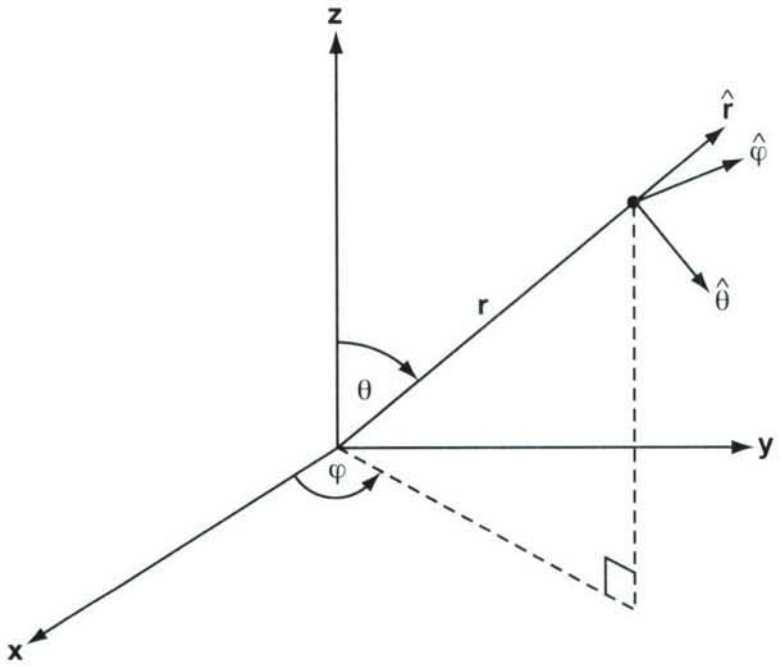

Figure 6-1. Spherical Coordinate System with Associated Unit Vectors ($\hat{r},\hat{\theta},\hat{\varphi}$)

Figure 6-2 show plots of the directive gain of each QHA element at its respective height above sea water that were determined from the measured free-space patterns given in figure 5-13. The directive gain patterns are similar to the free-space patterns for the co-polar component plotted in figure 5-13b except for the additional oscillations in the plots of figure 6-2. The added oscillations in the plots of figure 6-2 are attributed to multipath interference. The most noticeable differences between the corresponding element plots in figures 5-13a and 6-2 is at low elevation angles (i.e., in the vicinity of the air-sea water interface). In spite of the multipath interference observed in the element patterns above sea water, they appear to have an acceptable performance. The effect of buoy tilt on the element patterns and the analysis of several beamformers using the element patterns in figure 6-2 are addressed in reference 1.

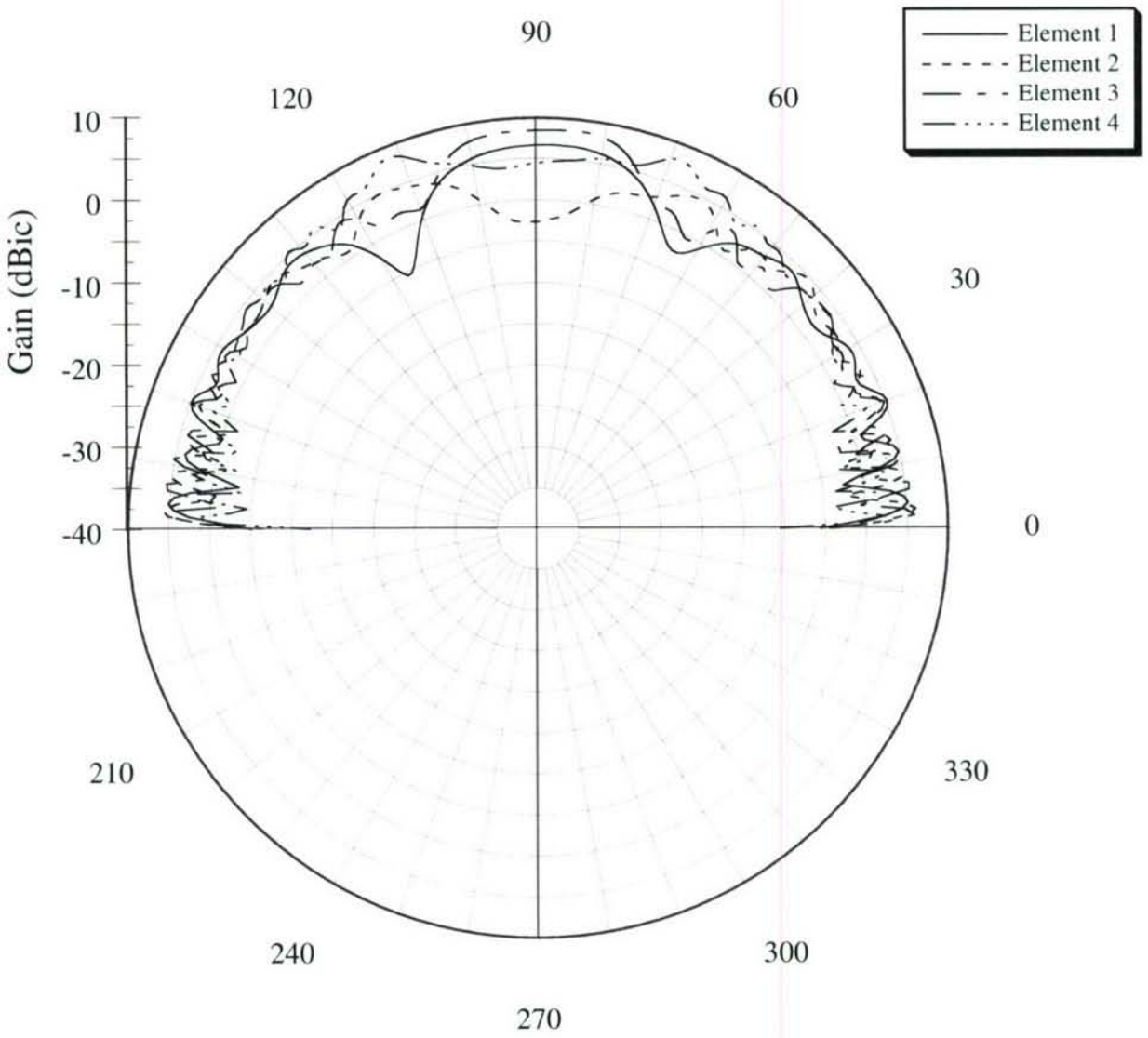

Figure 6-2. Directive Gain Patterns vs Elevation Angle of the QHA Elements Above Sea Water as Determined from the Measured Element Patterns in Free Space Shown in Figure 5-12

7. SUMMARY AND CONCLUSIONS

This report has provided a detailed description of the design of a linear array consisting of four QHAs that is to be installed on a buoy to support the transmission and reception of communication signals over LOS paths above the ocean surface over a narrow frequency bandwidth centered at 2.45 GHz. The measured radiation characteristics of the QHA elements in free space suggest that the array has good immunity to multipath interference and should have a satisfactory operation above a sea water half-space. The results of a sea test involving the array and buoy system are presented in another report by the authors (reference 1).

Although the feed design for this array is novel, it imposes several limitations that limit the performance of the QHA array. For example, the use of a brass tube that encloses the element feed cables required that the QHA elements have a sufficiently large diameter, resulting in a decrease in the element length-to-diameter ratio, thereby increasing the amount of radiation into the backside direction. To keep the brass tube sufficiently narrow so as not to significantly degrade the performance of each QHA element, thin coaxial cables with losses of 1.1 dB/ft at 2.45 GHz had to be used. Thinner coaxial cables have higher losses that reduce the antenna gain. The use of a narrow brass tube also restricted the maximum number of array elements to four, thereby limiting the maximum gain that can be achieved by a linear array of these QHAs.

An improvement in the array design may be obtained by placing the feed cables along the helical conductors (thin copper strips), thereby eliminating the need for a brass tube. This design would allow larger feed cables with smaller losses than the current cables and would permit a narrower QHA element design with improved circuit and radiation characteristics. This feed design would also permit a larger number of array elements, thereby increasing the gain of the array. However, one main issue with this design is regarding how to excite each QHA with equal power. In addition to a modification in the array feed design, the inclusion of an RF absorbing material on the top of the buoy plate should reduce undesirable reflections and improve the radiation characteristics of the array.

REFERENCES

1. J. P. Casey, S. M. Davis, M. J. Josypenko, and R. F. Ingram, "Multipath-Abating Antenna System for Line-of-Sight Communications Above an Air-Sea Water Interface," NUWC-NPT Technical Report (in preparation), Naval Undersea Warfare Center Division, Newport, RI (UNCLASSIFIED).

2. R. A. Burberry, "VHF and UHF Antennas," Ch. 17 in *The Handbook of Antenna Design*, vols. 1 and 2, A. W. Rudge, et al. (eds.), Peter Peregrinus Ltd., London, UK, 1986, pp. 1442-1443.

3. R. H. DuHamel and A. R. Mahnad, "TV and FM Transmitting Antennas," Ch. 28 in *Antenna Engineering Handbook*, Third Edition, R. C. Johnson (ed.), McGraw-Hill, New York, 1993, pp. 28-8 to 28-11.

4. C. C. Counselman, "Multipath-Rejecting GPS Antennas," *Proceedings of the IEEE*, vol. 87, no. 1, January 1999, pp. 86-91.

5. G. J. Burke, "Numerical Electromagnetics Code - NEC-4.1 - Method of Moments, Parts I and II," UCRL-MA-109338, Lawrence Livermore Laboratory, Livermore, CA, January 1992.

6. C. C. Counselman, private communication, 1 April 2004.

7. C. C. Kilgus, "Multielement, Fractional Turn Helices," *IEEE Transactions on Antennas and Propagation*, vol. AP-16, July 1968, pp. 499-501.

8. C. C. Kilgus, "Resonant Quadrifilar Helix Design," *Microwave Journal*, vol. 13, December 1970, pp. 49-54.

9. C. A. Balanis, *Antenna Theory: Analysis and Design*, Harper & Row, New York, 1982, pp. 43-46.

INITIAL DISTRIBUTION LIST

Addressee	No. of Copies
Office of Naval Research (K. Jenne, S. Das)	2
Space and Naval Warfare Command (PMW 770—J. Staggs, S. Valvonis)	2
University of Connecticut (R. Bansal)	1
Defense Technical Information Center	2